Response to referees: Chemical Characterisation of Water-soluble Ions in Atmospheric Particulate Matter on the East Coast of Peninsular Malaysia

The authors would like to thank each referee for their positive remarks about the paper and their interesting suggestions. The specific comments are addressed below.

Anonymous Referee #2
Received and published: 13 June 2018

The manuscript "Chemical Characterisation of Water-soluble Ions in Atmospheric Particulate Matter on the East Coast of Peninsular Malaysia" by Farren et al. investigated the particulate matters on the east coast of Peninsular Malaysia. Chemical components of particles (mainly soluble ions) were measured. Air mass trajectories were applied to indicate the potential source regions of various aerosol components. A thermodynamic model is used to estimate the aerosol acidity. Generally, this study revealed the characteristics of atmospheric chemistry over the East Coast of Peninsular Malaysia, which has been rarely reported. This manuscript served to fill in the gap of the Southeast Asia region which has been poorly characterized of its emissions, air quality, etc.

However, the chemical characteristics of aerosol over this region is not well studied. The design of the measurement is inadequate based on a Jan. – Feb. sampling of about thirty samples. No sampling during the biomass burning season is conducted.

Whilst we agree that our study is over a relatively short period, we feel that this work gives sufficient insight into the factors that affect aerosol composition to be suitable for publication in ACP. This study was not targeted at biomass burning but instead the impact of pollution outflow from Southeast Asia during very polluted periods.

The presentation of the data analysis (almost all the figures) is not good. Substantial revisions are suggested before this manuscript can be further reviewed. The major comments are list below: 1. Section 2: The method section should be reorganized. The sampling part should be described in the beginning of the section. Then the analytical procedures are presented. This study used quartz fiber filters for particle collection and the subsequent ion analysis. However, it is known that the quartz fiber filters have high background values of some cations such as Ca^{2+}, Mg^{2+}, etc. Did the authors perform ion analysis of the blank filters? What are the values of the ions of the blank filters?

The sample and extraction paragraph of the method section has been moved to the beginning of the section, followed by the analytical procedures.

As mentioned in section 2.4 (method validation), ion analysis of the blank filters has already been performed as part of this study. Blank subtractions were applied to any target ions found in detectable amounts. Procedural blank peak areas for each ion and average blank contribution to field samples over the entire sampling period are provided in the Supplement, Table S1.

Section 3.1 should be moved to the methodology section as it is related to the uncertainties of the chemical analysis but not the analysis results.

Section 3.1, which relates to the uncertainties of the chemical analysis, has been incorporated into section 2.4 (method validation).

Line 395 – 405: The description of ISOROPPIA-II should be moved to the Method Section.

The description of ISOROPPIA-II has been integrated into the method section (Section 2.6, ISOROPPIA-II model) and section 3.3.3 has been reworded accordingly.

2. Line 222 – 224: It is not appropriate to compare the results with the previous one as the study period is quite different. Furthermore, why don't use the concentrations of PM2.5 based on your data?

Concentrations of $PM_{2.5}$ based on our data are not available. These sentences were written to introduce the section on aerosol composition but are not essential for the study and have been removed.

3. Line 269 – 270: Is there any volcano activity during the study period. If not, this citation is not necessary.

There was no known volcanic activity during the study period. This sentence has been removed.

4. Line 287 – 288: The pollution rose plot (Fig. 6) cannot show the SO2 concentrations under calm conditions as the rose plot is based on conditions with wind speed higher than zero. Thus, the writings "The majority of higher SO2 events were observed in calm conditions when the air arriving at the site had passed over land to the south west of Bachok." is not based on sound analysis.

This observation has now been explained more carefully (lines 347-352). Figure 6 shows the relationship between wind direction and SO_2 concentration for SO_2 concentrations $\geq$ 5 ppb. In the bottom right corner, 'mean' represents the mean SO_2 concentration (20.1 ppb) and 'calm' represents the fraction of data that cannot be attributed to a specific wind direction (7.1%). The average wind speed during elevated ($\geq$ 5 ppb) SO_2 periods was 1.1 m s^{-1}. The average wind speed during the lower (< 5 ppb) SO_2 periods was considerably higher, 2.8 m s^{-1}.

5. Line 310 – 320: It is concluded that clusters 4 and 10 are associated with high SO42- concentrations of 20.4 and 18.1 μg m-3, respectively. It is understandable that cluster 4 passed over industrialized areas such as southern China and Southeast Asia, thus bringing considerable amounts of sulfate. However, it is explained that the high sulfate in cluster 10 is attributed to Manila First, it should be noted that the total emissions and emission intensity of Manila should be much lower than mainland China. Secondly, Cluster 10 travelled long distances over the ocean, which is supposed to have a clean effect on the aerosol concentrations.

In response to comments from referee #1, the cluster analysis has been reduced to 5 clusters and 7-day trajectories are reported (rather than 10-day) as they are more representative of the troposphere. Further analysis of this data shows that clusters 2, 3 and 5 are associated with the highest SO_4^{2-} concentrations, 14.4, 13.8 and 18.1 μg m^{-3} respectively. Clusters 2 and 3 passed over industrialised regions *e.g.* southern China and brought considerable amounts of sulfate. However, without additional measurements, the full reason for the high SO_4^{2-} levels in cluster 5 (same as cluster 10 in referee comment) is not clear. Interestingly, air masses within cluster 5 come from much higher altitudes than the other clusters and there is evidence of a low pressure system, generating anticlockwise winds around a possible cyclone in the South China Sea north of the island of Borneo. Cluster 5 only incorporates the final 24-hour period of the measurement campaign (06/02/2014 12:00 – 07/02/2014 12:00) and only one SO_4^{2-} measurement is available (18.1 μg m^{-3}). Further measurements of air masses similar to those in cluster 5 are needed to understand the high SO_4^{2-} levels. This section has been amended to provide a better explanation (lines 381-392).

6. What is the definition of chlorine-containing very short-lived substances (Cl-VSLSs)? What species are included as Cl-VSLSs? It seems that the authors regarded Cl-VSLSs as a tracer for anthropogenic emissions and use it for further analysis of SO42- during the pollution and less polluted periods. This is problematic as SO42- and Cl-VSLSs should have different origins and behaviour during the long-range transport, e.g. dry/wet deposition, decomposition rate.

Cl-VSLSs are ozone depleting species with short atmospheric lifetimes, typically less than 6 months. Species include dichloromethane (CH_2Cl_2) and 1,2-dichloroethane (CH_2ClCH_2Cl). The author agrees that SO_4^{2-} and Cl-VSLSs are likely to have different sources and atmospheric behaviour and that a direct comparison of these pollutants is not suitable. Nevertheless, this section is intended to demonstrate that there is additional evidence to support the observation that polluted air masses, containing a range of chemical pollutants, are being transported from East Asia to tropical regions of the western Pacific. This section (lines 406-419) has been rephrased to explain this more clearly.

7. Line 430 – 437: These paragraphs are basically not related to this study.

This paragraph puts the study into a wider context but has been shortened significantly (lines 520-530).

8. Line 474 – 475: As indicated by Fig. 4, the levels of K+ were less than 1ug/m3 throughout the whole study period, suggesting no significant biomass burning events. Thus, it is wrongly concluded that "biomass burning is a secondary source of oxalate".

Whilst the K^+ levels suggest that the measurement site was not heavily influenced by significant biomass burning events in the local area, the levels of K^+ do not rule out the influence of biomass burning on a regional/national scale. Biomass burning aerosol in the wider region will have undergone atmospheric processing and dispersion prior to arrival at the measurement site, potentially lowering K^+ levels and raising the concentration of secondary species. Due to both the strong correlation of oxalate and *nss*K^+, and the high oxalate/*nss*K^+ ratio, it is likely that biomass burning in the wider region has influenced the secondary formation of oxalate for example. The strong correlation with SO_4^{2-} and weak correlation with NO_3^- suggests that secondary oxalate formation has occurred through an aqueous phase oxidation process, for which biomass burning particles may have acted as cloud condensation nuclei. This section has been reworded to explain this point more clearly (lines 547-562).

9. Section 3.3.5: This section discussed about the Cl-/Na+ ratio and found the ratio was lower than its value of the seawater. It is concluded that the anthropogenic pollution via the long-range transport (Fig. 10) exerted the impact on the depletion of chloride. This is questionable as the study period is Jan. – Feb., which is the winter heating season in China. Based on Fig. 10, the air masses passed over vast areas of northern China, indicating aerosol rich in chloride from coal burning should be derived. If the monitoring site is influenced by emissions from China as discussed by this study, the Cl-/Na+ ratio should be much higher than 1.0.

It is possible that aerosol, particularly in northern China, may be rich in chloride in the winter due to coal burning. For example, our recent measurements at a ground-level urban background site in Beijing during Nov-Dec 2016 show average Cl^- levels of 6.3 μg m^{-3}. This is significantly higher than Cl^- concentrations at the Bachok measurement site, which were 0.67 μg m^{-3} on average during the measurement period. However, the air masses passed over regions of northern China at relatively high altitudes, exceeding 4000 m in some cases. In fact, figure 11 has been updated to show 7-day trajectories instead of 10-day trajectories in response to other referee comments, as these are more representative of the troposphere.

As shown in Figure 11, $Cl^-/ssNa^+$ molar ratios were less than 1.18 in all cases, showing significant Cl^- depletion. Greater Cl^- depletion was observed in continental air masses arriving at the site that had passed over industrialised regions in southern China, and Vietnam. The Cl^- depletion process has been studied extensively and it is widely accepted that Cl^- depletion can occur through the volatilization of HCl *via* acid displacement by nitric and sulfuric acid, particularly in relatively polluted marine air masses (Newberg et al., 2005; Sturges and Shaw, 1993). Whilst the air masses may be influenced by coal burning in China, they will also contain a vast mixture of other anthropogenic pollutants *e.g.* NO_x, SO_x, nitric acid and sulfuric acid. The presence of such pollutants means that as the air is transported over the South China Sea to the Bachok measurement site, there is potential for significant Cl^- depletion to occur. Lines 616 – 641 have been updated to explain this.

10. Line 522 – 523: It is hard to say that sulfate suppressed the formation of nitrate. The possible cause should be the deficiency of NH3, leading to the incomplete neutralization of sulfate and nitrate.

This section has been explained in more detail (lines 653-657). These measurements may be linked to each other through the important role of H_2SO_4 in the atmosphere. Acid displacement, when sea salt reacts with H_2SO_4, leads to the removal of Cl^- from the aerosol as gaseous HCl, and a partitioning of SO_4^{2-} to the aerosol as Na_2SO_4. Furthermore, under an ammonia-poor regime (as observed in this study), H_2SO_4 has a lower vapour pressure than HNO_3, leading to the preferential formation of ammonium sulfate over ammonium nitrate when there is insufficient NH_3 available to fully neutralize sulfate and nitrate (Seinfeld and Pandis, 2006).

Minor Comments:

Page 6, Line 191: Taiwan is not a country.

This sentence has been adjusted accordingly (line 245).

Line 204: Ashfold et al. ; Line 222: Dominick et al.; Line 322: Oram et al.; Line 445: Freitas et al.; Line 456: Carlton et al.; Line 466: Huang et al.; The format is incorrect.

The format of the in-text citations has been corrected.

Line 335: what does “a NAME trajectory” mean?

The UK Met Office’s Numerical Atmospheric Dispersion Modelling Environment (NAME) is used to model a range of atmospheric dispersion events. The full name has been provided in the text (line 424-426).

Anonymous Referee #1
Received and published: 15 June 2018

The manuscript by Farren et al. entitled as ‘Chemical Characterisation of Water-soluble Ions in Atmospheric Particulate Matter on the East Coast of Peninsular Malaysia’ presents the observation data at Malaysia. The method and data quality seem to be reasonably good. The data in the manuscript could be a good addition to the existing data set in the region. Quality of figures and descriptions could significantly be improved. I provide some comments related to the presentation quality below. It would be good if the authors could significantly improve it.

Comments

L45 ‘During the northern hemisphere winter, a large anticyclone forms over Siberia each year, creating strong north-easterly monsoon winds in the South China Sea (Northeast Monsoon). These strong north-easterlies can transport air masses from rapidly developing East Asian countries (e.g. China, Japan, Taiwan, Vietnam, North and South Korea) across the South China Sea to the Maritime Continent.

’ I am not sure if the statement is true. Please add references to support the description.

References have been added to support this statement (lines 48-49).

L185 ‘Figure 2 shows the 10-day backward air mass trajectories arriving at the measurement site during the demonstration campaign.’

Further details of the back-trajectory calculations, such as altitude, will be needed. It is not clear to me if a back trajectory analysis in the troposphere could provide a reliable result for such a long time-scale.

Further details of the back trajectories have been provided in the Supplement (Table S3). The back trajectories have been reduced to 7-day trajectories to better represent the troposphere. Figure 2 has been updated to colour the backward air mass trajectories by the altitude of the air mass.

L224 ‘and it is likely that the remainder was comprised primarily of organic aerosol’

Please provide a supporting information on this statement.

This sentence has been removed. It is not an important addition to the manuscript.

L240 ‘the mean Na+ /Ca2+ ratio in the crust and mean Ca2+ /Na+ ratio in seawater have been estimated as 1.78 w/w and 0.038 w/w respectively (Bowen, 1979)’ I wonder how stable these values are. The uncertainties in the values directly influence the following discussion. Please provide a detailed description, rather than simply referring one publication.

Na^+ and Ca^{2+} are both dominant cations in seawater with long residence times (1 million and 68 million years respectively). Although the total salt concentration or salinity of seawater varies somewhat, the ratio of the concentrations of major constituents to Cl^- are remarkably constant and the ocean is well-mixed (Bowen, 1979). There may be more uncertainty in the mean Ca^{2+}/Na^+ crustal ratio, as it is more challenging to predict the elemental composition of the crust. The ratio used in this study is based on the assumption that the crust consists of 50% basalt and 50% granite (Taylor, 1964). Despite potential uncertainties, as reported by Becagli et al. (2005) and Boreddy and Kawamura (2015), this approach provides greater accuracy than simply using total Na^+ as a sea-spray marker. Importantly, none of the overall trends are drastically altered by using this approach. For example, similar correlations are observed for oxalate and $nssSO_4^{2-}$ (R = 0.69) as oxalate and total SO_4^{2-} (R = 0.68) etc. Furthermore, ratios such as $Cl^-/ssNa^+$ are not hugely different to $Cl^-/totalNa^+$ (average molar ratios are 0.40 and 0.36 respectively). This has been explained more carefully in section 3.3.1 (lines 299-301).

L314 ‘Air masses in cluster 10 passed over the megacity of Manila in the Philippines, but may have slightly lower SO42- levels due to the height of the back trajectories;’

I am unable to judge if the statement is valid, as no information about altitude is provided in the manuscript.

Please refer to the response to comment 5 (referee #2).

L351 'The uptake of SO42- is preferential to the uptake of NO3- because sulfuric acid has a lower vapour pressure than nitric acid, and aqueous or solid (NH4)2SO4 is the preferred form of sulfate'
The statement is unclear to me. Please clarify.

This statement has been clarified (lines 441-443). The average NH_4^+/SO_4^{2-} molar ratio was 0.81, which indicated that there was insufficient gaseous NH_3 in the atmosphere to neutralise SO_4^{2-}. Under an ammonia-poor regime, the uptake of SO_4^{2-} is preferential to the uptake of NO_3^- because sulfuric acid has a lower vapour pressure than nitric acid (Seinfeld and Pandis, 2006).

L402 'The ambient temperature and relative humidity data were taken from the measurements made nearby at the Sultan Ismail Petra airport.'

It seems to me that the authors assumed an internal mixing state in using the thermodynamic model. Is there any supporting evidence on this assumption?

One of the key assumptions of ISOROPPIA-II is that particles are internally mixed. This may limit the accuracy of the pH prediction, in additional to other limitations, such as the lack of gaseous NH_3 and HNO_3 measurements. However, assuming the particles are internally mixed is not unreasonable for this study. Firstly, there is evidence that aerosol arriving at the Bachok research station is often aged and hence tends to be internally mixed. Secondly, relative humidity remained high throughout the study (average = 77%). A short discussion of the internal mixing state assumption has been incorporated into section 2.6 (lines 207-213).

Figure 7

Almost all the trajectories look similar to me, except for C10. Please provide the detailed reasoning for classification.

Cluster analysis is used on back trajectories to group similar air mass origins together. Back trajectories with similar geographic origin and grouped together to gain information on pollutant species with similar chemical histories. A distance matrix is used to created a required number of clusters (*e.g.* n = 5) with the most different air mass trajectories. This has been explained in lines 364-366. As shown in an updated version of Figure 7 (Figure 8), the cluster analysis has been altered so that fewer clusters are now used (n = 5). These clusters are sufficiently different enough, in terms of their geographic origin and altitude, to describe the effect of different air mass origins on pollutant species.

Minor comments

L76 'Dominick et al. characterised ..' I believe that it should be written as 'Dominick et al. (2015) characterized. . .' There are many similar descriptions when the authors cite other publications. Please check the recent publications of the journal carefully in preparing a manuscript.

The format of the in-text citations has been corrected throughout the text.

L200 ‘The station is located approximately 23 km away at the Sultan Ismail Petra airport in Kota Bharu (6.17298N, 102.2928E), as shown in Fig. S1 (Supplement)’

A similar information has already appeared at L150. Please minimize duplicated descriptions.

The duplication of this description has been minimized accordingly.

References

Becagli, S., Proposito, M., Benassai, S., Gragnani, R., Magand, O., Traversi, R., and Udisti, R.: Spatial distribution of biogenic sulphur compounds (MSA, nssSO(4)(2-)) in the northern Victoria Land-Dome C-Wilkes Land, area, East Antarctica, Ann Glaciol, 41, 23-31, Doi 10.3189/172756405781813384, 2005.
Boreddy, S. K. R., and Kawamura, K.: A 12-year observation of water-soluble ions in TSP aerosols collected at a remote marine location in the western North Pacific: an outflow region of Asian dust, Atmos Chem Phys, 15, 6437-6453, 10.5194/acp-15-6437-2015, 2015.
Bowen, H. J. M.: Environmental chemistry of the elements, Academic Press, London, 1979.
Newberg, J. T., Matthew, B. M., and Anastasio, C.: Chloride and bromide depletions in sea-salt particles over the northeastern Pacific Ocean, J Geophys Res-Atmos, 110, Artn D06209
10.1029/2004jd005446, 2005.
Seinfeld, J. H., and Pandis, S. N.: Atmospheric chemistry and physics : from air pollution to climate change, 2nd ed., J. Wiley, Hoboken, N.J., 1-1203 pp., 2006.
Sturges, W. T., and Shaw, G. E.: Halogens in Aerosols in Central Alaska, Atmos Environ a-Gen, 27, 2969-2977, Doi 10.1016/0960-1686(93)90329-W, 1993.
Taylor, S. R.: Abundance of Chemical Elements in the Continental Crust - a New Table, Geochim Cosmochim Ac, 28, 1273-1285, Doi 10.1016/0016-7037(64)90129-2, 1964.

Chemical Characterisation of Water-soluble Ions in Atmospheric Particulate Matter on the East Coast of Peninsular Malaysia

Naomi J. Farren[1], Rachel E. Dunmore[1], Mohammed Iqbal Mead[2], Mohd Shahrul Mohd Nadzir[3,4], Azizan Abu Samah[5], Siew-Moi Phang[5], William T. Sturges[6], Jacqueline F. Hamilton[1].

[1]Wolfson Atmospheric Chemistry Laboratories, Department of Chemistry, University of York, York, YO10 5DD, UK.
[2]Centre for Atmospheric Informatics and Emissions Technology, School of Energy, Environment and Agrifood/Environmental Technology, Cranfield University, Cranfield, UK.
[3]Centre for Tropical Climate Change System (IKLIM), Institute of Climate Change, Universiti Kebangsaan Malaysia, 43600 Bangi, Selangor, Malaysia.
[4]School of Environmental Science and Natural Resources, Faculty of Science and Technology, Universiti Kebangsaan Malaysia, 43600 Bangi, Selangor Darul Ehsan, Malaysia.
[5]Institute of Ocean and Earth Sciences, University of Malaya, Kuala Lumpur, Malaysia.
[6]Centre for Ocean and Atmospheric Sciences, School of Environmental Sciences, University of East Anglia, Norwich, UK.

Correspondence to: Jacqueline F. Hamilton (jacqui.hamilton@york.ac.uk)

Abstract.

Air quality on the east coast of Peninsular Malaysia is influenced by local anthropogenic and biogenic emissions, as well as marine air masses from the South China Sea and aged emissions transported from highly polluted East Asian regions during the winter monsoon season. An atmospheric observation tower has been constructed on this coastline at the Bachok Marine and Atmospheric Research Station. Daily $PM_{2.5}$ samples were collected from the top of the observation tower over a 3-week period, and ion chromatography was used to make time-resolved measurements of major atmospheric ions present in aerosol. SO_4^{2-} was found to be the most dominant ion present, and on average made up 66% of the total ion content. Predictions of aerosol pH were made using the ISOROPPIA-II thermodynamic model and it was estimated that the aerosol was highly acidic, with pH values ranging from -0.97 to 1.12. A clear difference in aerosol composition was found between continental air masses originating from industrialised regions of East Asia and marine air masses predominantly influenced by the South China Sea. For example, elevated SO_4^{2-} concentrations and increased Cl^- depletion was observed when continental air masses that had passed over highly industrialised regions of East Asia arrived at the measurement site. Correlation analyses of the ionic species and assessment of ratios between different ions provided an insight into common sources and formation pathways of key atmospheric ions, such as SO_4^{2-}, NH_4^+ and $C_2O_4^{2-}$. To our knowledge, time-resolved measurements of water-soluble ions in $PM_{2.5}$ are virtually non-existent in rural locations on the east coast of Peninsular Malaysia; overall this dataset contributes towards a better understanding of atmospheric composition in the Maritime Continent, a region of the tropics that is vulnerable to the effects of poor air quality, largely as a result of rapid industrialisation in East Asia.

1 Introduction

The tropical Maritime Continent, a region in Southeast Asia between 10° S – 20 °N and 90° - 150° E, is a complex distribution of islands and peninsulas, and incorporates countries such as Malaysia, Indonesia, the Philippines and Papua New Guinea (Neale and Slingo, 2003). It lies within a tropical warm pool that extends eastwards from the Indian Ocean to the Western Pacific, and is home to some of the warmest ocean temperatures in the world. Tropical regions such as the Maritime Continent are of central importance for the chemistry-climate system (Carpenter et al., 2010). For example, high photochemical activity in these regions means that global atmospheric lifetimes of key atmospheric species, such as methane and ozone, are controlled by destruction rates in the tropics (Lawrence et al., 2001; Bloss et al., 2005). In terms of ocean productivity, the observed decrease in primary productivity in low-latitude oceans has been linked to a reduced availability of nutrients for phytoplankton growth, caused by changes in upper-ocean temperature and stratification (Behrenfeld et al., 2006). Furthermore, the wind circulation system in the Maritime Continent is influenced by seasonal Asian monsoons, which are controlled by the natural oscillation of the intertropical convergence zone (ITCZ). During the northern hemisphere winter, a large anticyclone forms over Siberia each year, creating strong north-easterly monsoon winds in the South China Sea (Northeast Monsoon). These strong north-easterlies can transport air masses from rapidly developing East Asian countries (*e.g.* China, Japan, ~~Taiwan,~~ Vietnam, North and South Korea) across the South China Sea to the Maritime Continent (Zhang et al., 1997; Garreaud, 2001; Oram et al., 2017). In addition, cold surge events occur regularly throughout the winter monsoon season and last several days. Cold surges occur as a result of a south-easterly movement of the anticyclone, and are characterised by cold air masses over Southern China and strengthening of the north-easterly monsoon winds in the South China Sea (Zhang et al., 1997). The transport of pollution from East Asia to the tropics during the monsoon season, particularly during cold surges, means that rural areas such as the east coast of Peninsular Malaysia are potentially at an elevated risk of the detrimental effects of poor air quality.

Tropical regions are highly important for atmospheric research, and whilst long-term atmospheric observations exist (Robinson et al., 2014; Pyle et al., 2011), there are fewer measurements than in the mid and high-latitudes. The Bachok Marine and Atmospheric Research Station (6.00892° N, 102.42504° E) has been set up on the east coast of Peninsular Malaysia and is ideally located for studying the outflow of these highly industrialised regions, and for investigating the interaction with cleaner air in the Southern hemisphere. The research station forms part of the Institute of Ocean and Earth Sciences at the University of Malaya (UM), and is located approximately 30 km away from Kota Bharu. An atmospheric observation tower facing the South China Sea has been constructed at the research station; this has been built for the specific purpose of monitoring long-range transported pollution, air sea exchange and coastal meteorology. The research station is working towards designation as a regional Global Atmospheric Watch (GAW) centre, which will be a valuable addition to the network of other global and regional GAW sites in the Maritime Continent, as shown in Fig. 1 (gawsis.ch, 2017).

Figure 1: Location of global (green pins) and regional (blue pins) GAW sites in the Maritime Continent; Danum Valley in Malaysia (DMV), Bukit Kototabang in Indonesia (BKT), Manila in Philippines (MNI), Songkhla in Thailand (SKH), Tanah Rata in Malaysia (TAR), Petaling Jaya in Malaysia (PJM) and Singapore (SIN) (gawsis.ch, 2017). The red pin shows the location of the Bachok Marine and Atmospheric Research Station. Map created using google maps (google.com, 2017).

In January and February 2014, an instrument demonstration campaign was carried out to assess the capabilities of the new research station. This was funded by the Natural Environment Research Council (NERC) and UM and involved several UK universities, as well as the National Centre for Atmospheric Science (NCAS), UM and the Malaysia Meteorological Department (MMD). As part of this study, ~~Dunmore et al. used a specialised multi-dimensional gas chromatography technique to accurately measure atmospheric mixing ratios of C_5-C_{13} VOC species with a wide range of functionalities~~ Dunmore et al. (2016) used a specialised multi-dimensional gas chromatography technique to accurately measure atmospheric mixing ratios of C_5-C_{13} VOC species with a wide range of functionalities. Furthermore, ~~Dominick et al. characterised the particulate matter in Bachok by studying the influence of north-easterly winds on the patterns of particle mass and particle number concentration size distributions~~ Dominick et al. (2015) characterised the particulate matter in Bachok by studying the influence of north-easterly winds on the patterns of particle mass and particle number concentration size distributions. Both studies highlighted the fact that the site is influenced by a mixture of local anthropogenic and biogenic emissions, clean marine air masses, and aged emissions transported from East Asia.

To extend upon these studies, it is important to investigate atmospheric aerosol composition in the Bachok region. A better understanding of aerosol chemical composition is essential as aerosols play an important role in atmospheric processes and climate change. For example, aerosols can modify the global radiation budget both directly, by scattering and absorbing solar radiation, and indirectly, by altering cloud properties and lifetime (Charlson et al., 1991). The strength of these direct and indirect effects depends partly on the particle concentration and size distribution, but also on the chemical composition.

There are a limited number of studies that focus on particulate matter composition on the east coast of Peninsular Malaysia, and to our knowledge the composition of ionic species has not been determined at any rural locations along this coastline. For example, ~~Tahir et al. studied the composition of major elements and water-soluble ionic species in $PM_{2.5}$ and PM_{10} samples on the east coast of Peninsular Malaysia, but the samples were collected at an urban coastal city, Kuala Terengganu~~ Tahir et al. (2013) studied the composition of major elements and water-soluble ionic species in $PM_{2.5}$ and PM_{10} samples on the east coast of Peninsular Malaysia, but the samples were collected at an urban coastal city, Kuala Terengganu. This study used principal component analysis to determine the main sources of both fine and coarse particles, which were found to be soil dust, marine aerosol, vehicle exhaust, secondary aerosol, road dust and biomass burning. In addition, ~~Ismail et al. studied PM_{10} concentrations in three major cities (Kota Bahru, Kuala Terengganu and Kuantan) on the east coast of Peninsular Malaysia between 2006 and 2012~~ Ismail et al. (2016) studied PM_{10} concentrations in three major cities (Kota Bahru, Kuala Terengganu

and Kuantan) on the east coast of Peninsular Malaysia between 2006 and 2012. The study showed that during the Northeast Monsoon, the air arriving at the sites had originated from China and the Philippines and travelled over the South China Sea. During the Southwest Monsoon, the air came from Indonesia *via* the Straits of Malacca. Over the 6-year period, it was found that the atmospheric PM_{10} mass was directly proportional to the rate of urbanization in each of the three cities.

In this study, measurements of water-soluble ions in atmospheric aerosol at a rural coastal location on the east coast of Peninsular Malaysia are presented. Analysis of temporal variation of different ionic species has been carried out, and backward air mass trajectories have been used to determine the influence of air mass origin on aerosol composition. Correlation analyses of the ionic species and assessment of ratios between different ions has provided an insight into common sources and formation pathways of key atmospheric ions.

2 Experimental

2.1 Sample collection and extraction

Thirty $PM_{2.5}$ samples were collected at the Bachok Marine and Atmospheric Research Station (6.00892° N, 102.42504° E) between 18-01-2014 and 06-02-2014. The samples were collected at the top of an atmospheric observation tower (18 m height) using a high volume air sampler (Ecotech HiVol 3000, Victoria, Australia) operating at 1.13 m^3 min^{-1} over 24 h sampling intervals. The tower is located on the coastline of the South China Sea and is within 100 m of the shore. A 3-day intensive measurement period was in operation between midday (local time) on 30-01-2014 and midday on 02-02-2014, in which filters were collected every 4-8 hours. The quartz fibre filters (20.3 × 25.4 cm) supplied by Whatman (Maidstone, UK) were prebaked at 550 °C for a minimum of 12 h prior to sample collection. After sample collection, the filters were wrapped in aluminium foil and stored at -18 °C until analysis. To prepare the samples for analysis, 5.7 cm^2 of each sample was dissolved in 2 mL milli-Q water and sonicated for 30 min at room temperature. The extract was filtered using a Millex-GP 33 mm diameter hydrophilic syringe filter with a pore size of 0.22 µm (Millipore UK Limited, Watford, UK) and made up to a final volume of 2.5 mL.

2.2~~1~~ Eluents and analytical standards

Ultrapure milli-Q water (18 MΩ cm^{-1}) from an ELGA LabWater purification system was used to prepare all the required eluents and analytical standards. A 20 mM solution of methanesulfonic acid was used as the eluent for cation exchange chromatography and for anion exchange chromatography, a solution of 8 mM Na_2CO_3/1 mM $NaHCO_3$ was prepared. Using a variety of salts and organic acids, individual analytical standards containing 500 ppm of each target ion (Cl^-, NO_2^-, NO_3^-, PO_4^{3-}, SO_4^{2-}, $CH_3SO_3^-$, $C_2O_4^{2-}$, Na^+, NH_4^+, K^+, Mg^{2+} and Ca^{2+}) were prepared in milli-Q water. The salts and organic acids were purchased from either Sigma-Aldrich Ltd. (Dorset, UK) or Fisher Scientific Ltd. (Loughborough, UK).

Formatted: Normal

~~**2.2 Method validation**~~

~~Recovery tests were performed by spiking 5.7 cm^2 of quartz fibre filters (Whatman, Maidstone, UK) with 1 µg of each target ion (20 µL of a 50 ppm mixed ion solution). Prior to spiking, the filters were prebaked at 550 °C for 6 hours and wrapped in aluminium foil and stored at -18 °C until required. The spiked filters were dissolved in 2 mL of milli-Q water and sonicated for 30 min at room temperature. The extract was filtered using a Millex-GP 33 mm diameter hydrophilic syringe filter with a pore size of 0.22 µm (Millipore UK Limited, Watford, UK) and made up to a final volume of 2.5 mL. Procedural blanks were also carried out using quartz fibre filters (5.7 cm^2) and blank subtractions were applied to any target ions found in detectable amounts.~~

~~**2.3 Sample collection and extraction**~~

~~Thirty $PM_{2.5}$ samples were collected at the Bachok Marine and Atmospheric Research Station (6.00892° N, 102.42504° E) between 18-01-2014 and 06-02-2014. The samples were collected at the top of an atmospheric observation tower (18 m height) using a high volume air sampler (Ecotech HiVol 3000, Victoria, Australia) operating at 1.13 m^3 min^{-1} over 24 h sampling intervals. The tower is located on the coastline of the South China Sea and is within 100 m of the shore. A 3-day intensive measurement period was in operation between midday (local time) on 30-01-2014 and midday on 02-02-2014, in which filters were collected every 4-8 hours. The quartz fibre filters (20.3 × 25.4 cm) supplied by Whatman (Maidstone, UK) were prebaked at 550 °C for a minimum of 12 h prior to sample collection. After sample collection, the filters were wrapped in aluminium foil and stored at -18 °C until analysis. To prepare the samples for analysis, 5.7 cm^2 of each sample was dissolved in 2 mL milli-Q water and sonicated for 30 min at room temperature. The extract was filtered using a Millex-GP 33 mm diameter hydrophilic syringe filter with a pore size of 0.22 µm (Millipore UK Limited, Watford, UK) and made up to a final volume of 2.5 mL.~~

2.~~4~~ ~~3~~ Chromatographic analysis

Chromatographic analysis was carried out using a Thermo Scientific Dionex ICS-1100 ion chromatography system equipped with an AS-DV autosampler. The column configuration used for anion exchange consisted of an IonPac AG14A guard column (4 × 50 mm) and an IonPac AS14A analytical column (4 × 250 mm). Cation exchange chromatography was performed using an IonPac CG12A guard column (4 × 50 mm) and an IonPac CS12A analytical column (4 × 250 mm). ASRS 300 and CSRS 300 self-regenerating suppressors (4 mm) were used for anion and cation exchange respectively. All columns and suppressors were supplied from Thermo Scientific Dionex. The run times for the anion and cation separations were 18 and 15 min respectively. The suppressor current was 45 mA for anion exchange mode, and 59 mA for cation exchange mode. For all separations, the instrument was operated in isocratic mode at a flow rate of 1 mL min^{-1} and a column oven temperature of 30 °C. The injection volume was 100 µL and the data collection rate was 5 Hz. The system relied on a DS6 heated conductivity

cell for ion detection and all data was analysed using Thermo Scientific Chromeleon 7.1 Chromatography Data System software.

2.4 Method validation

Using isocratic elution methods for both cation and anion exchange chromatography, the target ions were successfully separated. Recovery tests were performed by spiking 5.7 cm^2 of quartz fibre filters (Whatman, Maidstone, UK) with 1 µg of each target ion (20 µL of a 50 ppm mixed ion solution). Prior to spiking, the filters were prebaked at 550 °C for 6 hours and wrapped in aluminium foil and stored at -18 °C until required. The spiked filters were dissolved in 2 mL of milli-Q water and sonicated for 30 min at room temperature. The extract was filtered using a Millex-GP 33 mm diameter hydrophilic syringe filter with a pore size of 0.22 µm (Millipore UK Limited, Watford, UK) and made up to a final volume of 2.5 mL. The recovery of the target ions from the filter papers ranged from 74.5% to 98.2% for the target anions, and 78.3% to 87.3% for the target cations, with the exception of Ca^{2+} for which a recovery level of 123.3% was calculated. Recovery tests were carried out in triplicate and $\%RSD_{rec}$ remained below 8% for all the ions. The recovery of Ca^{2+} should not have exceeded 100% and the result may be attributed to inconsistencies in the amount of Ca^{2+} present on the blank filter, or due to Ca^{2+} contamination during sample collection or storage. 100% recovery was assumed for Ca^{2+} during the data analysis process. Further details of the individual recovery levels and associated errors can be found in the Supplement (Table S1). Procedural blanks were also carried out using quartz fibre filters (5.7 cm^2) and blank subtractions were applied to any target ions found in detectable amounts. The blank peak areas for each ion and average blank contribution to field samples over the entire sampling period are provided in the Supplement, Table S1. The main instrumental parameters of the IC system were evaluated and are also detailed in the Supplement (Table S2). Instrumental limits of detection (LODs) and limits of quantification (LOQs) were calculated according to the EPA protocol 40 CFR 136; multiplying the standard deviation (N = 10, 5 ng for cations, 25 ng for anions) by the Student t-value (N = 10, 95% confidence interval) gave the LOD, and multiplying the standard deviation by 10 gave the LOQ (EPA, 2017; Ripp, 1996). For anion exchange chromatography, LODs and LOQs were in the range 5.5 – 21.0 ng and 25.3 – 144.2 ng respectively. For cation exchange chromatography, the LODs ranged from 0.5 to 2.1 ng and the LOQs ranged from 2.5 to 6.1 ng. On average, the instrument precision ($\%RSD_{ins,}$ n = 10) was 4.2% for the target cations and 12.8% for the target anions. Total errors were estimated by combining errors with the instrument and the recovery process and remained below 15.4% for all ions except NO_3^- (22.6%).

2.5 Additional measurements

Individual volatile organic compounds (VOCs) were measured using a combined heart-cut and comprehensive two-dimensional gas chromatography system (GC-GC×GC); a detailed description of the instrument design is provided in a separate study (Dunmore et al., 2016). Measurements of NO and NO_2 were performed using a two channel TE42i commercial gas analyser (Thermo Scientific, MA, USA), and SO_2 measurements were made using a Thermo Scientific 43i SO_2 ~~analyser.~~ analyser. Meteorological data from the nearest meteorological station, the Sultan Ismail Petra Airport (6.17208° N,

102.29288° E), ~~Meteorological data~~ was accessed from the Integrated Surface Database (NOAA, 2003). ~~The data selected was from the nearest meteorological station, approximately 23 km away from the Bachok measurement site at the Sultan Ismail Petra Airport (6.17208° N, 102.29288° E).~~ Hourly measurements of wind direction, wind speed, air temperature, dew point, atmospheric pressure and relative humidity were obtained. 10-day backward air mass trajectories arriving at the sampling site were run every 3 hours throughout the entire measurement period. A receptor height of 10 m was chosen to represent the measurements made on the sampling tower. The trajectories were computed using the Hybrid Single-Particle Lagrangian Integrated Trajectory (HYSPLIT) model (Stein et al., 2015; Draxler, 1999; Draxler and Hess, 1998, 1997), and the data was analysed using the openair package in RStudio (Carslaw and Ropkins, 2012; Carslaw, 2015).

2.6 ISORROPIA-II model

Predictions of aerosol pH were made using the ISORROPIA-II thermodynamic equilibrium model. Although these models produce better results when gas phase measurements such as NH_3 and HNO_3 are available, it is possible to use the ion measurements obtained in this study to make a prediction of aerosol pH (Fountoukis and Nenes, 2007). Calculations were made in 'reverse mode', in which known quantities are temperature, relative humidity, and particle phase concentrations of NH_4^+, SO_4^{2-}, Na^+, Cl^-, NO_3^-, Ca^{2+}, K^+ and Mg^{2+}. ISOROPPIA-II assumes that the particles are internally mixed; this is a reasonable assumption for this study, as relative humidity was high (average = 77%) and the aerosol arriving at the measurement site is often aged. The aerosol was assumed to be thermodynamically stable, *i.e.* the aerosol can exist as both solid and liquid, and salts are able to precipitate if the aqueous phase becomes saturated with respect to them. The ambient temperature and relative humidity data were taken from the measurements made nearby at the Sultan Ismail Petra airport. It is likely that these measurements are representative of the Bachok research station, as further investigation of data from two other meteorological stations showed that temperature and relative humidity remain consistent along the coastline. ~~The aerosol was assumed to be thermodynamically stable *i.e.* the aerosol can exist as both solid and liquid, and salts are able to precipitate if the aqueous phase becomes saturated with respect to them.~~

Formatted: Don't keep with next
Formatted: Subscript
Formatted: Subscript
Formatted: Font: Italic
Formatted: Font:

3 Results and discussion

~~3.1 Method validation~~

~~Using isocratic elution methods for both cation and anion exchange chromatography, the target ions were successfully separated. The recovery of the target ions from the filter papers ranged from 74.5% to 98.2% for the target anions, and 78.3% to 87.3% for the target cations, with the exception of Ca^{2+} for which a recovery level of 123.3% was calculated. Recovery tests were carried out in triplicate and $\%RSD_{rec}$ remained below 8% for all the ions. The recovery of Ca^{2+} should not have exceeded 100% and the result may be attributed to inconsistencies in the amount of Ca^{2+} present on the blank filter, or due to Ca^{2+} contamination during sample collection or storage. 100% recovery was assumed for Ca^{2+} during the data analysis process. All~~

~~the reported ion concentrations in this study have been corrected for procedural blanks. Further details of the individual recovery levels and associated errors, as well as the blank contribution of each ion can be found in the Supplement (Table S1). The main instrumental parameters of the IC system were evaluated and are also detailed in the Supplement (Table S2). Instrumental limits of detection (LODs) and limits of quantification (LOQs) were calculated according to the EPA protocol 40 CFR 136; multiplying the standard deviation (N = 10, 5 ng for cations, 25 ng for anions) by the Student t-value (N = 10, 95% confidence interval) gave the LOD, and multiplying the standard deviation by 10 gave the LOQ (EPA, 2017; Ripp, 1996). For anion exchange chromatography, LODs and LOQs were in the range 5.5 – 21.0 ng and 25.3 – 144.2 ng respectively. For cation exchange chromatography, the LODs ranged from 0.5 to 2.1 ng and the LOQs ranged from 2.5 to 6.1 ng. On average, the instrument precision ($\%RSD_{ins}$, n = 10) was 4.2% for the target cations and 12.8% for the target anions. Total errors were estimated by combining errors with the instrument and the recovery process and remained below 15.4% for all ions except NO_3^- (22.6%). In summary, the IC method proved to be a reliable technique, allowing for water-soluble ions in atmospheric aerosol to be quantified accurately.~~

3.~~2~~1 Bachok demonstration campaign

The filter samples were collected at the Bachok atmospheric observation tower. The Bachok district, located in the state of Kelantan, is a rural area and the primary economic activity comes from tobacco and kenaf plantations. Other agrarian activities in the wider Kelantan region include the production of rice and rubber, as well as additional economic activities such as livestock rearing and fishing. Figure 2 shows the ~~10~~7-day backward air mass trajectories arriving at the measurement site during the demonstration campaign, coloured by the altitude of the air mass (m). As expected during the winter months, the strong anticyclone system known as the Siberian High led to the arrival of north-easterly onshore winds along the east coast of Peninsular Malaysia. Some of the air masses experienced a significant continental influence from highly industrialised countries such as China, ~~Japan, Taiwan and North~~Japan, North and South Korea and the island of Taiwan, ~~,~~ whilst other air masses had a stronger marine influence from both the East China Sea and the South China Sea.

Figure 2: ~~10~~7-day HYSPLIT backward air mass trajectories centred on the Bachok Marine and Atmospheric Research Station between 18-01-2014 and 07-02-2014. The back trajectories are coloured by the altitude of the air mass (m). **Plot constructed using the openair package in RStudio (Carslaw and Ropkins, 2012; Carslaw, 2015).**

Although there was no reliable meteorological data recorded at the measurement site during the demonstration campaign, data from a nearby meteorological station was available. The station is located approximately 23 km away at the Sultan Ismail Petra airport in Kota Bharu ~~(6.17298° N, 102.29288° E)~~, as shown in Fig. S1 (Supplement). Whilst the meteorological data from the airport will not be exactly representative of the measurement site, the patterns in wind direction are consistent with observations made by the field scientists during the campaign. In addition, during a study of the influence of Northeast Monsoon cold surges on air quality in Southeast Asia, ~~Ashfold et al. used meteorological data from three locations that they believed to lie in the~~

path of cold surges during the Northeast Monsoon, offering the best possibility of observing a cold surge influence on air pollution Ashfold et al. (2017) used meteorological data from three locations that they believed to lie in the path of cold surges during the Northeast Monsoon, offering the best possibility of observing a cold surge influence on air pollution. These sites were in Kota Bharu (102.247° E, 6.141° N), Kuala Terengganu (103.118° E, 5.308° N) and Kemaman (103.428° E, 4.271° N); this provides further confirmation that data from the Sultan Ismail Petra airport site is suitable for evaluating broad scale transport at the Bachok measurement site. Fig. S2 in the Supplement shows average hourly wind speed and wind direction conditions across the entire duration of the measurement campaign (18-01-2014 to 06-02-2014). On most days, gentle south westerlies from the land (Peninsular Malaysia) were observed in the early hours of the morning, through to around 11 am. At this stage, a dramatic shift in wind direction occurred, and until around 19:00 a strong onshore breeze from the north east (South China Sea) was observed. From 20:00 to the early hours of each morning, a calmer sea breeze predominantly from the east was seen. Hourly VOC measurements were conducted at the measurement site, and the development of a sea breeze at approximately 11:00 dramatically influenced the diurnal profiles of the measured species (Fig. S3, Supplement). In the morning, when the air being sampled was coming over the land, high levels of NO, NO_2 and anthropogenic VOCs such as toluene and C_{10} aliphatics were observed; the main source of these species was local burning of waste (Dunmore et al., 2016). When the sea breeze developed the concentration of these species dropped significantly.

3.3 Composition of water-soluble ions in atmospheric aerosol

3.3.1 Aerosol composition and determination of non-sea salt and sea salt components

The total concentration of measured water-soluble ions in the $PM_{2.5}$ during the campaign ranged from 8.06 to 27.0 μg m^{-3}, with an average concentration of 16.2 μg m^{-3}. A study of particle mass and number concentration at the Bachok measurement site was carried out by Dominick et al.; average $PM_{2.5}$ and PM_{10} concentrations of 30 μg m^{-3} and 31 μg m^{-3} were observed respectively between 09-01-2014 and 23-03-2014 Dominick et al. (2015). This data suggests that on average, the measured water-soluble ions in this study made up approximately half of the total $PM_{2.5}$, and it is likely that the remainder was comprised primarily of organic aerosol. During the measurement campaign, PM levels regularly exceeded the WHO $PM_{2.5}$ guidelines for the 24-hour mean (25 μg m^{-3}) (WHO, 2006). Table 1 shows the mean and maximum water-soluble ion concentrations measured throughout the campaign, and Figures 3 and 4 show time series for all the ions measured in the aerosol.

Table 1: Mean and maximum ion concentrations measured throughout the measurement period. The average % mass contribution of each ion to the total measured ions is included, as well as the % of samples in which each target ion is found (%Qt).

Figure 3: Time series of SO_4^{2-}, NH_4^+, Na^+, Cl^-, NO_3^- and NO_2^- concentration (μg m^{-3}) during the Bachok demonstration campaign (18-01-2014 to 07-02-2014). Yellow shaded areas represent the time between sunrise and sunset (local).

Figure 4: Time series of PO_4^{3-}, Ca^{2+}, Mg^{2+}, K^+, $C_2O_4^{2-}$ and $CH_3SO_3^-$ concentration (µg m^{-3}) during the Bachok demonstration campaign (18-01-2014 to 07-02-2014). Yellow shaded areas represent the time between sunrise and sunset (local).

As the composition of the water-soluble ions present in aerosol collected at the Bachok site was influenced by both marine and continental sources, it is useful to make an estimation of non-sea salt (*nss*) and sea salt (*ss*) components, using Eq. (1) – Eq. (4). Total Na^+ and Ca^{2+} concentrations have been measured in this study, and the mean Ca^{2+}/Na^+ ratio in the crust and mean Ca^{2+}/Na^+ ratio in seawater have been estimated as 1.78 *w/w* and 0.038 *w/w* respectively (Bowen, 1979). Therefore is it possible to solve Eq. (1) – Eq. (4) simultaneously for *ss*Na^+, *nss*Na^+, *ss*Ca^{2+} and *nss*Ca^{2+} (Boreddy and Kawamura, 2015). Furthermore, the resulting estimate of *ss*Na^+, which can be used as a sea spray marker, can also be used to predict the contribution of *nss*SO_4^{2-} and *nss*K^+ in the aerosol, as shown in Eq. (5) and Eq. (6) respectively. Whilst there may be some uncertainty in the mean Ca^{2+}/Na^+ crustal ratio, due to challenges associated with predicting the composition of the crust (Bowen, 1979), this approach provides more accuracy than simply using total Na^+ as a sea spray marker.

Formatted: Superscript

Formatted: Superscript

Formatted: Superscript

Formatted: Superscript

$$ssNa^+ = Na^+ - nssNa^+ \quad (1)$$

$$nssNa^+ = nssCa^{2+} \cdot \left(\frac{Ca^{2+}}{Na^+}\right)_{crust} \quad (2)$$

$$nssCa^{2+} = Ca^{2+} - ssCa^{2+} \quad (3)$$

$$ssCa^{2+} = ssNa^+ \cdot \left(\frac{Ca^{2+}}{Na^+}\right)_{sea\ water} \quad (4)$$

$$nssSO_4^{2-} = SO_4^{2-} - 0.253 \cdot ssNa^+ \quad (5)$$

$$nssK^+ = K^+ - 0.037 \cdot ssNa^+ \quad (6)$$

Figure 5 shows a series of pie charts to summarise the average mass composition of water-soluble ions in atmospheric aerosol, and the distribution of non-sea salt and sea salt components. The results show that the water-soluble ion fraction of the aerosol is dominated by SO_4^{2-}, which on average made up 65.6% of the total ion content by mass. NH_4^+ and NO_3^- concentrations were significantly lower, with mean concentrations of 1.69 and 0.61 µg m^{-3} respectively. Na^+ and Cl^- made up 11.1% of the total ion content, and 75% of the measured Na^+ was attributed to *ss*Na^+. The average concentrations of *nss*K^+ and *nss*Ca^{2+} were 0.30 and 0.09 µg m^{-3} respectively; these ions can be used as tracers for biomass burning (*nss*K^+) and atmospheric dust (*nss*Ca^{2+}). NO_2^- and $CH_3SO_3^-$ were the least abundant ions, with average concentrations of 0.05 and 0.08 µg m^{-3}. The two ions were only observed in a subset of samples; $CH_3SO_3^-$ was quantified in 67% of samples and quantification of NO_2^- was only achieved in 23% of samples.

Figure 5: Pie chart to show the average composition of water-soluble ions in aerosol collected at the Bachok research station (upper panel) and pie charts to show the percentage of non-sea salt and sea salt fractions of Na^+, SO_4^{2-}, K^+, Ca^{2+} (lower panel, left to right).

3.3.2 Sources and formation of sulfate (SO_4^{2-})

The average SO_4^{2-} concentration during the measurement campaign was 10.7 μg m^{-3}, with a maximum concentration of 20.8 μg m^{-3} recorded. The formation of SO_4^{2-} in the particle phase occurs when emitted SO_2 is oxidised by OH in the gas phase, or by O_3 or H_2O_2 in the aqueous phase (Fisher et al., 2011). The most dominant anthropogenic sources of SO_2 include fuel and industrial emissions, as well as open biomass burning. ~~Natural sources of SO_2 arise from both volcanic activity and the oxidation of biogenic dimethyl sulphide (DMS) (Fisher et al., 2011).~~

By using *ss*Na^+ as a sea spray marker to determine non-sea salt and sea salt components of the aerosol, it was found that on average 96% of the measured SO_4^{2-} was *nss*SO_4^{2-}, and only 4% of the SO_4^{2-} was from sea salt. As a potential biogenic source of *nss*SO_4^{2-} is DMS emissions from marine biota, and the main atmospheric source of MSA is the oxidation of DMS, it is possible to use the MSA^-/*nss*SO_4^{2-} ratio as a tracer to assess the contribution of biogenic sources to *nss*SO_4^{2-} in the atmosphere (Legrand and Pasteur, 1998). In this study, MSA^- concentrations ranged from 0.02 to 0.22 μg m^{-3}, with an average concentration of 0.08 μg m^{-3}. As a result, the MSA^-/*nss*SO_4^{2-} ratio ranged from ~~2.5~~1.6×10^{-4}~~$^{-3}$~~ to ~~2.3~~2.2×10^{-3}~~^{2}~~, with an average value of ~~7.8~~8.0×10^{-4}~~^{3}~~. These values are ~~very~~ low compared to MSA^-/*nss*SO_4^{2-} ratios recorded at remote sites; for example, a MSA^-/*nss*SO_4^{2-} mean mass ratio of ~~0.0~~7×10^{-2} has been measured on Fanning Island and American Samoa (Savoie and Prospero, 1989). The lower ratios recorded in Bachok suggest the majority of *nss*SO_4^{2-} at the site originates from anthropogenic sources.

As previously discussed, a study by ~~Dunmore et al. revealed that levels of NO_x and anthropogenic VOCs at the Bachok measurement site were significantly higher when the air being sampled had passed over nearby land, and dropped significantly at around 11 am when a sea breeze developed~~ Dunmore et al. (2016) revealed that levels of NO_x and anthropogenic VOCs at the Bachok measurement site were significantly higher when the air being sampled had passed over nearby land, and dropped significantly at around 11 am when a sea breeze developed. This indicated that air quality in Bachok is influenced by local sources of pollution, such as vehicle emissions and burning domestic waste. A pollution rose is shown in Fig. 6 to show the relationship between gaseous SO_2 and wind direction. SO_2 concentrations below 5 ppb have been excluded in order to investigate the wind conditions when the spikes in SO_2 concentration occur in more detail. In the lower right corner of the plot, 'mean' represents the mean SO_2 concentration (20.1 ppbv) and 'calm' represents the fraction of data that cannot be attributed to a specific wind direction (7.1%). During these elevated (≥ 5 ppbv) SO_2 periods, weak south westerlies dominated and the average wind speed was 1.1 m s^{-1}. A different situation was observed during the lower (< 5 ppbv) SO_2 periods; average wind speed was considerably higher, 2.8 m s^{-1}, and the air arrived predominantly from the east. In summary, the~~The~~ majority of higher SO_2 events were observed in calmer conditions when the air arriving at the site had passed over land to the south west of Bachok; this provides further evidence that the site is influenced by local sources of pollution.

Figure 6: Pollution rose to show the relationship between wind direction and SO_2 concentration (≥ 5 ppb) at the Bachok measurement site. Plot constructed using the openair package in RStudio (Carslaw and Ropkins, 2012; Carslaw, 2015).

Formatted: Superscript

Formatted: Subscript

Formatted: Superscript

Formatted: Subscript

Formatted: Superscript

At the Bachok measurement site, no obvious relationship was observed between SO_2 and particulate SO_4^{2-} concentration, or between SO_4^{2-} concentration and wind direction. This is likely to be because it takes time for SO_2 to oxidise to SO_4^{2-}, and that the SO_4^{2-} fraction of the aerosol is more heavily influenced by long-range transport of aged emissions from East Asia. To investigate this further, the backward air mass trajectories were coloured by the concentration of SO_4^{2-}, as shown in Fig. 7 (upper panel). The plot clearly shows that the SO_4^{2-} content of the aerosol is highest (*ca.* 14 – 20 µg m^{-3}) when the site is influenced by continental air masses from regions of East Asia, and lowest when the air masses have a more significant marine influence. With this information in mind, it is useful to perform cluster analysis on the back trajectories; this type of analysis groups air masses of similar geographic origin together, which provides more information on pollutant species with similar chemical histories. A distance matrix is used to create a specified number of clusters with the most different air mass pathways. Figure 8~~7 (lower panel)~~ shows the ~~10~~5-cluster solution to back trajectories calculated for the Bachok site during the measurement campaign.

Figure 7: 7-day HYSPLIT backward air mass trajectories centred on the Bachok research station between 18-01-2014 and 07-02-2014. The back trajectories are coloured by the concentration of SO_4^{2-} (µg m^{-3}). Plot constructed using the openair package in RStudio (Carslaw and Ropkins, 2012; Carslaw, 2015).

Figure 8: 5-cluster solution to backward air mass trajectories centred on the Bachok research station between 18-01-2014 and 07-02-2014. Plot constructed using the openair package in RStudio (Carslaw and Ropkins, 2012; Carslaw, 2015).

Formatted: Caption, Line spacing: 1.5 lines

~~**Figure 7: Upper panel shows 10-day HYSPLIT backward air mass trajectories centred on the Bachok research station between 18-01-2014 and 07-02-2014. The back trajectories are coloured by the concentration of SO_4^{2-} (µg m^{-3}). Lower panel shows the 10-cluster solution to backward air mass trajectories centred on the Bachok research station during the same time period. The clusters are coloured by the average concentration of SO_4^{2-} (µg m^{-3}). Plot constructed using the openair package in RStudio (Carslaw and Ropkins, 2012; Carslaw, 2015).**~~

Clusters 2 and 3 were associated with mean SO_4^{2-} concentrations of 14.4 and 13.8 µg m^{-3} respectively. The mean altitude of cluster 2 was 65 m and the mean altitude of cluster 3 was 501 m. Full details of the air mass trajectories within each cluster are detailed in the Supplement (Table S3). These clusters contained air masses that had passed over several highly industrialised regions en route to Bachok, including cities such as Zhanjiang (China) and Ho Chi Minh City (Vietnam). Average SO_4^{2-} concentrations for clusters 1 and 4 were 8.4 and 8.3 µg m^{-3}, with mean altitudes of 169 and 37 m respectively. These air masses may have experienced some continental influence from the east coast of China but mainly passed over the South China Sea before arriving at Bachok. Air masses within cluster 5 had a mean altitude of 1000 m and the SO_4^{2-} concentration was 18.1 µg m^{-3}. The air masses within this cluster came from much higher altitudes, and there is evidence of a low pressure system, generating anticlockwise winds around a possible cyclone in the South China Sea north of Borneo. Cluster 5 only incorporates the final 24-hour period of the measurement campaign (06/02/2014 12:00 – 07/02/2014 12:00) and only one SO_4^{2-}

Formatted: Subscript
Formatted: Superscript
Formatted: Superscript
Formatted: Subscript
Formatted: Superscript
Formatted: Superscript
Formatted: Subscript
Formatted: Superscript
Formatted: Superscript
Formatted: Subscript
Formatted: Superscript

measurement is available (18.1 µg m^{-3}). Further measurements are needed under similar conditions in order to fully understand the nature of air masses from this region. ~~The air masses associated with the highest SO_4^{2-} content are represented by clusters 4 and 10 shown in the lower panel of Fig. 7; average SO_4^{2-} concentrations for these two clusters were 20.4 and 18.1 µg m^{-3} respectively. Cluster 4 contained air masses that had passed over several highly industrialised regions en route to Bachok, including cities such as Zhanjiang (China) and Ho Chi Minh City (Vietnam). Air masses in cluster 10 passed over the megacity of Manila in the Philippines, but may have slightly lower SO_4^{2-} levels due to the height of the back trajectories; the average height (above sea level) of the back trajectories in cluster 4 was 181 m over the 10 day period, whilst the average height for the trajectories in cluster 10 was 1575 m. Average SO_4^{2-} concentrations for clusters 1, 3 and 5 were 11.5, 14.1 and 10.5 µg m^{-3} respectively. These air masses experienced some continental influence from the east coast of China but mainly passed over the South China Sea before arriving at Bachok. Air masses with the lowest average SO_4^{2-} content (between 6.6 and 8.7 µg m^{-3}) were associated with clusters 2 and 6 – 9. Most of these air masses originated from the East China Sea and South China Sea and did not undergo any significant continental influence.~~

~~Similar observations have been reported in a separate study by Oram et al., in which chlorine-containing very short-lived substances (Cl-VSLSs) were measured at the Bachok research station during the same winter monsoon season in late January/ early February 2014.~~ Further evidence that substantial amounts of industrial pollution from East Asia are undergoing atmospheric transport to tropical regions of the western Pacific is provided in a separate study by Oram et al. (2017). Chlorine-containing very short-lived substances (Cl-VSLSs) were measured at the Bachok research station during the winter monsoon season in late January/ early February 2014. Cl-VSLSs are ozone depleting species with short atmospheric lifetimes, typically less than 6 months. Species include dichloromethane (CH_2Cl_2) and 1,2-dichloroethane (CH_2ClCH_2Cl). A 7-day pollution or cold-surge event was reported between 19-01-2014 and 26-01-2014, when significantly enhanced concentrations of Cl-VSLSs were observed. During this pollution episode, the measured samples were heavily impacted by emissions from the East Asian mainland, whilst this influence was less significant during the cleaner, non-polluted periods. In fact, the total median concentration of the four measured Cl-VSLSs was 546 ppt between 20 and 26 Jan, and 243 ppt during the less polluted period (27-01-2014 to 05-02-2014). ~~In this study, the mean SO_4^{2-} concentrations in these two periods were 14.9 and 8.8 µg m^{-3} respectively. Furthermore,~~ Oram et al. (2017) noted that even after the cold surge event, the levels of Cl-VSLSs were still significantly higher than expected, indicating that this region of the South China Sea is widely impacted by emissions from East Asia. Many other chemical pollutants, aside from short-lived chlorinated gases, will be present in these air masses from East Asia and will have a large impact on regional air quality. ~~The widespread influence from industrial emissions on a regional scale is further evidenced in this study. For example, whilst air masses arriving at Bachok from highly industrialised regions contained higher SO_4^{2-} levels, the SO_4^{2-} concentration remained above 5 µg m^{-3} throughout the entire measurement period. To further investigate the frequency and duration of the pollution or cold surge events, Oram et al. performed a NAME trajectory analysis using carbon monoxide (CO) as a tracer of industrial emissions from regions north of 20° N for 6 winter seasons (2009/2010 – 2014/2015)~~ Oram et al. (2017) performed a Numerical Atmospheric Dispersion Modelling Environment

Formatted: Superscript

Formatted: Subscript

Formatted: Subscript

Formatted: Subscript

Formatted: Subscript

(NAME) trajectory analysis using carbon monoxide (CO) as a tracer of industrial emissions from regions north of 20° N for 6 winter seasons (2009/2010 – 2014/2015). A strong correlation between CO and CH_2Cl_2 (a measured Cl-VSLS) was observed during the pollution episode in late January 2014. Analysis of CO time series over the 6 winter seasons revealed that cold surge events are likely to be repeated regularly each winter, demonstrating that pollution rapidly undergoes long-range transport across the South China Sea on a regular basis during the Northeast Monsoon.

3.3.3 Correlation of SO_4^{2-} with NH_4^+ and implications for aerosol acidity

Ammonium (NH_4^+) was the second most abundant ion in the aerosol; on average it made up 10.4% of the total ion content, and mean and maximum concentrations were 1.69 and 4.73 μg m^{-3} respectively. Strong positive correlation between SO_4^{2-} and NH_4^+ was observed ($R = 0.776$, $p < 0.001$). A similar observation was reported by ~~Keywood et al. during an investigation of the sources of particles contributing to haze in the Klang Valley, Malaysia~~ Keywood et al. (2003) during an investigation of the sources of particles contributing to haze in the Klang Valley, Malaysia. The strong relationship between these species is due to neutralisation of SO_4^{2-} by NH_4^+. It is likely that NH_3 emissions in the rural Bachok region come predominantly from agricultural practices such as animal husbandry, fertilizer use and agricultural waste burning. The measurement site is possibly influenced by other key NH_3 sources included in the Emissions Database for Global Atmospheric Research (EDGAR), such as direct soil emissions and road transport, but it is difficult to ascertain which sources are most dominant as the database does not provide local/ regional scale NH_3 emissions data for Malaysia (edgar.eu, 2016).

The average NH_4^+/SO_4^{2-} molar ratio was 0.81, which indicated that there was insufficient gaseous NH_3 in the atmosphere to neutralise SO_4^{2-}. Under an ammonia-poor regime, ~~T~~the uptake of SO_4^{2-} is preferential to the uptake of NO_3^- because sulfuric acid has a lower vapour pressure than nitric acid~~, and aqueous or solid $(NH_4)_2SO_4$ is the preferred form of sulfate~~ (Seinfeld and Pandis, 2006). ~~The average NH_4^+/SO_4^{2-} molar ratio was 0.81, which indicated that there was insufficient gaseous NH_3 in the atmosphere to neutralise SO_4^{2-}.~~ Although measurements of the total amounts of ammonia and sulfate in the gas, aqueous and solid phase would provide a better prediction of the aerosol acidity, the results presented in this study indicated that an ammonia-poor regime exists, and that the aerosol is likely to be acidic. In these scenarios, the NH_3 partial pressure is low, and therefore the NH_3-HNO_3 partial pressure product is also low, meaning that the concentrations of ammonium nitrate are low or zero (Seinfeld and Pandis, 2006). This hypothesis can be supported by the fact that NO_3^- concentrations in this study were very low, ranging from 0.005 to 1.52 μg m^{-3}. As a result, NO_3^- made up a significantly smaller fraction of the total ion content compared to SO_4^{2-}; average percentage mass composition of the total ion content was 3.8% for NO_3^- and 65.6% for SO_4^{2-}.

To estimate proton loading in atmospheric particles, the strong acidity approach can be used, as shown in Eq. (7). This approach assumes that any deficit in measured cation charge compared to measured anion charge can be attributed to H^+. Total anion and total cation equivalents can be estimated using Eq. (8) and Eq. (9).

$$strong\ acidity\ (\mu eq.m^{-3}) = \sum anion\ equivs.\ (\mu eq.m^{-3}) - \sum cation\ equivs.\ (\mu eq.m^{-3}) \quad (7)$$

$$\sum anion\ equivs.\ (\mu eq.m^{-3}) = \frac{SO_4^{2-}}{48} + \frac{NO_3^-}{62} + \frac{Cl^-}{35.5} + \frac{PO_4^{3-}}{31.6} + \frac{C_2O_4^{2-}}{44} + \frac{NO_2^-}{46} + \frac{CH_3SO_3^-}{95} \quad (8)$$

$$\sum cation\ equivs.\ (\mu eq.m^{-3}) = \frac{Na^+}{23} + \frac{NH_4^+}{18} + \frac{K^+}{39} + \frac{Mg^{2+}}{12} + \frac{Ca^{2+}}{20} \quad (9)$$

As shown in Fig. ~~8~~9, strong acidity values ranged from 0.03 to 0.19 µeq. m^{-3}, with an average value of 0.11 µeq. m^{-3}. The positive strong acidity values provide an initial indication that the aerosol is acidic and allows an estimate of the proton loading to be made (average H^+ = 0.11 µg m^{-3}).

Figure ~~8~~9: Particle strong acidity and associated error predictions for the aerosol collected during the Bachok measurement campaign. Yellow shaded areas represent the time between sunrise and sunset (local).

To obtain error bars for the strong acidity predictions (Fig. ~~8~~9), H^+_{max} and H^+_{min} were calculated according to Eq. (10) and Eq. (11) respectively. For H^+_{max} the anions were adjusted up to within their uncertainties (*i.e.* +%RSD_{tot}) and the cations were adjusted down to within their uncertainties (*i.e.* -%RSD_{tot}). For H^+_{min} the anions were adjusted down and the cations were adjusted up (Murphy et al., 2017). %RSD_{tot} was estimated by combining the error of the recovery process for each ion (%RSD_{rec}, Table S1) and the error of the instrument for each ion (%RSD_{ins}, Table S2).

$$H^+_{max} = \sum max.anion\ equivalents - \sum min.\ cation\ equivalents \quad (10)$$

$$H^+_{min} = \sum min.anion\ equivalents - \sum max.cation\ equivalents \quad (11)$$

In most cases, H^+_{min} remains above zero. However, between 02-02-2014 and 06-02-2014, slightly negative H^+_{min} values between -1×10^{-3} and -2×10^{-2} µeq. m^{-3} were calculated, which are physically implausible (Murphy et al., 2017). These results highlight the possible sources of error associated with the strong acidity approach for estimating aerosol acidity. For example, ~~Hennigan et al. report that organic acids (which are mostly excluded from this study, except for MSA and oxalic acid) can have an important influence on aerosol acidity, especially at relatively low acidities where organic acids dissociate and contribute to the ion balance~~ Hennigan et al. (2015) report that organic acids (which are mostly excluded from this study, except for MSA and oxalic acid) can have an important influence on aerosol acidity, especially at relatively low acidities where organic acids dissociate and contribute to the ion balance. Furthermore, they can form salt complexes with inorganic species *e.g.* ammonium oxalate. Neglecting organic acids, as well as other atmospheric species such as HCO_3^- and basic amines, will lead to inaccuracies in the calculated H^+.

Thermodynamic equilibrium models such as ISOROPPIA-II can also be used to predict aerosol pH. The ambient temperature and relative humidity data recorded nearby at the Sultan Ismail Petra airport were assumed representative of the Bachok

research station, as further investigation of data from two other meteorological stations revealed that temperature and relative humidity remained consistent.

~~The ambient temperature and relative humidity data were taken from the measurements made nearby at the Sultan Ismail Petra airport. It is likely that these measurements are representative of the Bachok research station, as further investigation of data from two other meteorological stations revealed that temperature and relative humidity remain consistent along the coastline.~~ A map to show the location of the three meteorological stations along the east coast, as well as the Bachok research station, can be found in the Supplement (Fig. S4). The two other stations are Narathiwat airport (6.520° N, 101.743° E) and Sultan Mahmud airport (5.383° N, 103.103°E). Average relative humidity between 18-01-2014 and 07-02-2014 was 77.7% at Sultan Petra Ismail airport, 75.4% at Narathiwat airport and 77.0% at Sultan Mahmud airport. Average temperatures recorded at the stations during this time were 24.8, 25.6 and 25.4 °C for Sultan Petra Ismail, Sultan Mahmud and Narathiwat airport respectively.

The ISOROPPIA-II thermodynamic model predictions of $PM_{2.5}$ pH are shown in Fig. ~~9~~10. Particle pH was estimated with ISOROPPIA-II run in the reverse mode without gas phase species input, and ranged from -0.97 to 1.12 during the measurement period, implying that the aerosol was highly acidic. The pH prediction for the aerosol collected between midday on 03-02-2014 and 04-02-2014 was 7.06 and has been excluded from Fig. ~~9~~10. The particle concentrations input on this day correspond to negative values of strong acidity and therefore the model balances charge by assuming $[OH^-] > [H^+]$; this leads to a calculated pH of greater than 7. Murphy et al. (2017) have reported that pH prediction is sensitive to strong acidity in the limit of strong acidity approaching zero and that the model can be drastically improved if gas phase NH_3 and HNO_3 measurements are included. The gas-to-particle partitioning of these species is sensitive to pH under conditions commonly encountered in the atmosphere, therefore gaseous NH_3 and HNO_3 measurements provide better constraint on the thermodynamic model.

Figure 109: Predicted $PM_{2.5}$ pH at the Bachok measurement site using ISOROPPIA-II. Yellow shaded areas represent the time between sunrise and sunset (local).

Acidic particles can have detrimental effects on human health, air quality, and the health of aquatic and terrestrial ecosystems (Hennigan et al., 2015). For example, ~~Gwynn et al. performed a time-series analysis of acidic PM and daily mortality and morbidity in the Buffalo, New York region; several significant pollutant-health effect associations were identified, the strongest being the correlation between atmospheric SO_4^{2-} concentration and respiratory hospital admissions~~ Gwynn et al. (2000) performed a time-series analysis of acidic PM and daily mortality and morbidity in the Buffalo, New York region; several significant pollutant-health effect associations were identified, the strongest being the correlation between atmospheric SO_4^{2-} concentration and respiratory hospital admissions. Furthermore, ~~Deposition of acidic gases and particles can affect the acid-neutralizing capacity of freshwater ecosystems, leading to biological damage and loss of invertebrates in worst-case scenarios (Schindler, 1988). The extent to which sulfate aerosol is neutralised also has important implications for aerosol~~

~~radiative forcing and ice cloud nucleation (Charlson et al., 1987). For example, estimates of the radiative forcing for anthropogenic sulfate aerosol range from -0.26 to -0.82 W m^{-2} (Graf et al., 1997). P~~particle acidity can influence various atmospheric chemical processes, including SO_2 oxidation, halogen chemistry, and the partitioning of ammonia, nitric acid, organic acids and isomeric epoxy diols from isoprene photooxidation (IEPOX) (Hennigan et al., 2015; Surratt et al., 2010; Lin et al., 2012). In summary, whilst some of the risks associated with aerosol acidity in Bachok originate from local sources of pollution, it is possible that people living in these rural areas are also exposed to an additional risk, as the region appears to be sensitive to the effects of industrialisation further afield in East Asia.

3.3.4 Sources and formation of oxalate, $C_2O_4^{2-}$

Oxalic acid is the most abundant dicarboxylic acid in tropospheric aerosol (Sareen et al., 2016). This major water-soluble organic component can alter the hygroscopicity of aerosols, and can either act as cloud condensation nuclei (CCN), or reduce the surface tension of particles to form CCN (Saxena and Hildemann, 1996; Novakov and Penner, 1993; Facchini et al., 1999; Kerminen, 2001). In this study, oxalate made up 2.6% of the total measured water-soluble ion content. The average concentration was 0.42 µg m^{-3}, and throughout the measurement period the concentration ranged from 0.15 to 0.65 µg m^{-3}. Interestingly, such levels of oxalate in atmospheric aerosol are typical of urban environments, despite the fact that the Bachok research station is located in a rural coastal region. For example, ~~Freitas et al. report average oxalate concentrations in TSP at an urban site and a rural site in Londrina City, Brazil of 0.57 and 0.03 µg m^{-3} respectively~~ Freitas et al. (2012) report average oxalate concentrations in TSP at an urban site and a rural site in Londrina City, Brazil of 0.57 and 0.03 µg m^{-3} respectively. Other reported oxalate concentrations in urban TSP include measurements of 0.10 – 0.48 µg m^{-3} in Shanghai (Jiang et al., 2011) and 0.27 µg m^{-3} in Tokyo (Sempere and Kawamura, 1994).

To investigate possible oxalate sources and formation pathways, it is necessary to consider the correlation of oxalate with different atmospheric species. ~~Jiang et al. report using NO_2^- as an indicator for vehicle emissions, *nss*SO_4^{2-} and NO_3^- for secondary formation through different pathways, and K^+ for biomass burning~~ Jiang et al. (2011) report using NO_2^- as an indicator for vehicle emissions, *nss*SO_4^{2-} and NO_3^- for secondary formation through different pathways, and K^+ for biomass burning. A study carried out by Huang et al. (2006) in the urban area of Shenzen (Southern China) reported that whilst good correlation of droplet oxalate with K^+ was observed (R^2 = 0.75, average diameter = 1.0 µm), there was poor correlation between oxalate and K^+ in the condensation mode (R^2 = 0.10, average diameter = 0.4 µm). This implied that whilst biomass burning was probably not an important primary source of condensation mode oxalate, it is likely that biomass burning particles act as effective CCN, promoting in-cloud sulfate and oxalate formation. In this study, *nss*K^+ levels remained below 0.7 µg m^{-3}, suggesting that the local area was influenced by dispersed biomass burning particles rather than at the measurement site itself. However, a strong correlation was observed between oxalate and *nss*K^+ (R = 0.78, $p < 0.001$), and therefore the oxalate/*nss*K^+ ratio was used to predict whether biomass burning on a regional/national scale was an important primary or secondary source of oxalate. ~~oxalate correlated strongly with *nss*K^+ (R = 0.65, $p < 0.001$). The oxalate/*nss*K^+ ratio was used to predict whether~~

Formatted: Font: Italic
Formatted: Superscript
Formatted: Superscript
Formatted: Font: Italic
Formatted: Superscript
Formatted: Font: Italic
Formatted: Superscript

~~biomass burning was an important primary or secondary source of oxalate.~~ The oxalate/*nss*K^+ ratio ranged from ~~0.49~~0.68 to ~~0.99~~4.64 during the Bachok demonstration campaign, significantly higher than those found in aerosol directly emitted from vegetation fires in the Amazon Basin (Yamasoe et al., 2000). This suggests that biomass burning in the region influenced the~~is an important~~ secondary ~~source~~formation of oxalate ~~in the Bachok region~~, rather than acting as a primary source of oxalate. ~~significant primary source.~~ A similar hypothesis was proposed by Huang and Yu (2007), who measured ambient $PM_{2.5}$ in an urban environment in the Pearl River Delta Region of China, and reported oxalate/K^+ ratios of 0.57 and 0.33 in summer and winter respectively. It is worth noting that whilst the higher ratios reported in both studies indicate that biomass burning is not a major primary source of oxalate, measurements of oxalate and K^+ in local biomass burning aerosols (rather than aerosol in the Amazon Basin) would provide a better indication of the source contribution by biomass burning.

There was no significant correlation observed between oxalate and NO_3^-, or between oxalate and NO_2^-. The lack of correlation with NO_3^- suggests that the two species do not have similar formation pathways, and that vehicle emissions are not an important secondary source of oxalate. It is also unlikely that vehicle emissions contribute to the primary sources of oxalate, due to the lack of correlation between oxalate and NO_2^-. However, NO_2^- was only detected in 7 out of the 30 samples collected, so it is difficult to ascertain whether there is a relationship between these two species or not.

Strong correlation between oxalate and *nss*SO_4^{2-} ($R = 0.69$, $p < 0.001$) was observed, suggesting a common formation pathway of the two species.~~In this study, there was a relatively strong correlation between oxalate and *nss*SO_4^{2-} ($R = 0.60$, $p < 0.001$), suggesting a common formation pathway of the two species.~~ It is well known that SO_4^{2-} forms *via* aqueous oxidation (Seinfeld and Pandis, 2006), and modelling studies also suggest that aqueous chemistry is a large contributor of oxalate formation globally (Myriokefalitakis et al., 2011). Furthermore, ~~Carlton et al. report that whilst there are likely to be many sources of oxalate, oxidation of pyruvate in the aqueous phase is known to form oxalate at dilute (cloud-relevant) concentrations~~ Carlton et al. (2006) report that whilst there are likely to be many sources of oxalate, oxidation of pyruvate in the aqueous phase is known to form oxalate at dilute (cloud-relevant) concentrations. ~~Tan et al. also state that aqueous acetate oxidation is a key source of oxalate~~ Tan et al. (2012) also state that aqueous acetate oxidation is a key source of oxalate. A positive correlation between oxalate and NH_4^+ was also observed ($R = 0.73$~~66~~, $p < 0.001$). A similar observation was reported by ~~Jiang et al. in a study of aerosol oxalate in Shanghai~~ Jiang et al. (2011) in a study of aerosol oxalate in Shanghai. Using size distribution data, they were able to propose that the correlation was due to the presence of ammonium oxalate in the aerosol. In this study there is no size distribution data available, and so it is important to consider the fact that the correlation may be linked to the influence of sulfate on both NH_4^+ and oxalate in aerosol; NH_4^+ partitions to the aerosol from gaseous NH_3 in an attempt to neutralise acidic sulfate particles, whilst oxalate exhibits similar formation pathways to SO_4^{2-}.

~~A study carried out by Huang et al. in the urban area of Shenzen (Southern China) reported that whilst good correlation of droplet oxalate with K^+ was observed ($R^2 = 0.75$, average diameter = 1.0 μm), there was poor correlation between oxalate and K^+ in the condensation mode ($R^2 = 0.10$, average diameter = 0.4 μm) Huang et al. (2006). This implied that whilst biomass~~

Formatted: Font: Italic

Formatted: Subscript

Formatted: Superscript

~~burning was probably not an important primary source of condensation mode oxalate, it is likely that biomass burning particles act as effective CCN, promoting in-cloud sulfate and oxalate formation. In this study, oxalate correlated strongly with *nss*K^+ ($R = 0.65$, $p < 0.001$). The oxalate/*nss*K^+ ratio was used to predict whether biomass burning was an important primary or secondary source of oxalate. The oxalate/*nss*K^+ ratio ranged from 0.49 to 0.99 during the Bachok demonstration campaign, significantly higher than those found in aerosol directly emitted from vegetation fires in the Amazon Basin (Yamasoe et al., 2000). This suggests that biomass burning is an important secondary source of oxalate in the Bachok region, rather than a significant primary source. A similar hypothesis was proposed by Huang et al., who measured ambient $PM_{2.5}$ in an urban environment in the Pearl River Delta Region of China, and reported oxalate/K^+ ratios of 0.57 and 0.33 in summer and winter respectively Huang and Yu (2007). However, it is worth noting that whilst the higher ratios reported in both studies indicate that biomass burning is not a major primary source of oxalate, measurements of oxalate and K^+ in local biomass burning aerosols (rather than aerosol in the Amazon Basin) would provide a better indication of the source contribution by biomass burning.~~

~~There was no significant correlation observed between oxalate and NO_3^-, or between oxalate and NO_3^-. The lack of correlation with NO_3^- suggests that the two species do not have similar formation pathways, and that vehicle emissions are not an important secondary source of oxalate. It is also unlikely that vehicle emissions contribute to the primary sources of oxalate, due to the lack of correlation between oxalate and NO_3^-. However, NO_3^- was only detected in 7 out of the 30 samples collected, so it is difficult to ascertain whether there is a relationship between these two species or not.~~

3.3.5 Sea salt aerosol and factors affecting chloride depletion

On average, Na^+ and Cl^- contributed 7.0% and 4.1% to the total measured water-soluble ion content respectively, and 72% of the measured Na^+ was attributed to *ss*Na^+. The concentration of *ss*Na^+ ranged from 0.24 to 2.35 μg m^{-3}, whilst the concentration of Cl^- ranged from 0.003 to 2.38 μg m^{-3}. There was no correlation between *nss*Na^+ and Cl^- ($R = -0.01$), but a strong positive correlation between *ss*Na^+ and Cl^- was observed ($R = 0.83$~~84~~, $p < 0.001$). During the measurement period, the $Cl^-/ssNa^+$ molar ratio ranged from 0.003 to 1.10 with an average value of 0.40. A time series of $Cl^-/ssNa^+$ molar ratio can be found in the Supplement (Fig. S5). Significant Cl^- depletion was observed, as all~~All~~ of the ratios recorded were lower than that of bulk seawater, 1.18 (Boreddy and Kawamura, 2015). Figure ~~10~~ 11 shows backward air mass trajectories arriving at the Bachok research station, coloured by the $Cl^-/ssNa^+$ molar ratio. ~~The plot shows that the lowest $Cl^-/ssNa^+$ ratios are found when continental air masses from highly industrialised countries such as China and Vietnam arrive at the site, and higher $Cl^-/ssNa^+$ ratios are found when marine air masses from the South China Sea arrive.~~

Formatted: Superscript

Figure ~~10~~11: ~~10~~7-day HYSPLIT back trajectories centred on the Bachok research station, between 18-01-2014 and 07-02-2014. The back trajectories are coloured by the $Cl^-/ssNa^+$ molar ratio. Plot constructed using the openair package in RStudio (Carslaw and Ropkins, 2012; Carslaw, 2015).

~~The relationship between $Cl^-/ssNa^+$ molar ratio and air mass origin shown in Fig. 10 clearly indicates that the extent of chloride depletion is greater when the aerosol has been more influenced by anthropogenic sources of pollution.~~ A study of marine aerosol at remote Chichijima Island in the western North Pacific during 2001 and 2002 reported that mean Cl^-/Na^+ molar ratios were highest (1.34) in September 2001 and lowest (0.30) in May 2002, and the mean ratio across the 2-year period was 1.10 (Boreddy et al., 2014). Boreddy et al. (2014) reported that the observed chloride depletion was likely due to acid displacement occurring as a result of atmospheric mixing of anthropogenic pollutants such as SO_x and NO_x. Acid displacement can occur when sea salt particles react with acids such as H_2SO_4, HNO_3, oxalic acid ($C_2H_2O_4$) and methanesulfonic acid (CH_3SO_3H) in the atmosphere. Such processes are of atmospheric importance as they lead to the formation of gaseous HCl and potentially affect acid deposition conditions in the region. It is widely accepted that Cl^- depletion through the volatilization of HCl *via* acid displacement occurs particularly in polluted marine air masses (Newberg et al., 2005; Sturges and Shaw, 1993). In this study, the lowest $Cl^-/ssNa^+$ ratios were observed when air masses arriving at the site had previously passed over highly industrialised countries such as China and Vietnam (Figure 11). Higher $Cl^-/ssNa^+$ ratios are found when the marine air masses are from less polluted regions. It is possible that aerosol, particularly in northern China, may be rich in chloride in the winter due to coal burning. However, this study suggests that the influence of other anthropogenic pollutants, such as HNO_3 and H_2SO_4, means that as the air is transported over the South China Sea to the Bachok region, significant Cl^- depletion can occur prior to arrival at the measurement site. In a more recent study, Boreddy and Kawamura performed regression analysis between the Cl^-/Na^+ mass ratio and various acidic species, including $nssSO_4^{2-}$, NO_3^-, MSA^- and oxalic acid. They found a moderate negative correlation between Cl^-/Na^+ mass ratio and $nssSO_4^{2-}$, and a moderate to weak negative correlation with NO_3^-; this suggested that sulfate had a higher influence on chloride depletion than nitrate. Furthermore, whilst MSA^- moderately correlated with the Cl^-/Na^+ mass ratio in the summer, there was significant negative correlation between oxalic acid and the mass ratio in the other three seasons, providing confirmation that oxalic acid plays an important role in chloride loss at Chichijima Island. A similar regression analysis was carried out on the measurements obtained during the Bachok measurement campaign, and whilst a weak negative correlation was found between SO_4^{2-} and the $Cl^-/ssNa^+$ mass ratio ($R = -0.41$, $p < 0.001$), there was no correlation of the $Cl^-/ssNa^+$ mass ratio with oxalate or MSA^-. These results imply that whilst H_2SO_4 played an important role in chloride depletion, methanesulfonic acid and oxalic acid may not have done. Interestingly, a strong positive correlation was observed between NO_3^- and $Cl^-/ssNa^+$ mass ratio ($R = 0.78.82$, $p < 0.001$). ~~This correlation may be explained by the fact that the high sulfate content of the aerosol in Bachok is capable of suppressing both NO_3^- and Cl^- levels.~~ These measurements may be linked to each other through the important role of H_2SO_4 in the atmosphere. Acid displacement, when sea salt reacts with H_2SO_4, leads to the removal of Cl^- from the aerosol as gaseous HCl, and a partitioning of SO_4^{2-} to the aerosol as Na_2SO_4. Furthermore, under an ammonia-poor regime (as observed in this study), H_2SO_4 has a lower vapour pressure than HNO_3, leading to the preferential formation of ammonium sulfate over ammonium nitrate when there is insufficient NH_3 available to fully neutralize sulfate and nitrate (Seinfeld and Pandis, 2006).

Formatted: Superscript
Formatted: Font: Italic
Formatted: Superscript
Formatted: Font: Italic
Formatted: Superscript
Formatted: Superscript
Formatted: Font: Italic
Formatted: Superscript
Formatted: Subscript
Formatted: Subscript
Formatted: Subscript
Formatted: Superscript
Formatted: Subscript
Formatted: Subscript
Formatted: Subscript
Formatted: Superscript
Formatted: Subscript
Formatted: Superscript
Formatted: Subscript
Formatted: Subscript
Formatted: Subscript
Formatted: Subscript
Formatted: Subscript
Formatted: Subscript

3.3.6 Using *nss*Ca^{2+} as a potential tracer for dust episodes

NssCa^{2+} can be used as a tracer for atmospheric dust (Boreddy and Kawamura, 2015). The average concentration of *nss*Ca^{2+} during the measurement campaign was 0.07 µg m^{-3} and the maximum concentration recorded was 0.28 µg m^{-3}. On most days, the *nss*Ca^{2+} concentration was below 0.10 µg m^{-3}, but between midday on 30-01-2014 and midnight on 31-01-2014 (local times), elevated *nss*Ca^{2+} levels were observed and the average concentration during this period was 0.22 µg m^{-3}. The same trend was observed for PO_4^{3-}; the average concentration across the entire measurement period was 0.34 µg m^{-3}, but during this 12-hour episode the PO_4^{3-} concentration increased to 1.88 µg m^{-3}. The increase in ion concentration was less pronounced for *nss*Na^{+} and Mg^{2+}, but the concentrations were still 0.26 and 0.88 µg m^{-3} above the average for the whole measurement period respectively. Time series plots for *nss*Ca^{2+}, PO_4^{3-}, Mg^{2+} and *nss*Na^{+} can be found in the Supplement (Figure S6).

Between midday on 30-01-2014 and midnight on 31-01-2014, *nss*Ca^{2+} contributed significantly (1.26%) to the total measured water-soluble ion content compared to the average contribution during the remainder of the measurement period (0.35%). The Bachok research station is located in the outflow region of Asian dusts, and these measurements suggest that long-range transport of Asian dusts over the measurement site has occurred during this time. In fact, during this episode, the back trajectories arriving at the site can be traced back to the North China Plains and the Horqin Sandy Land in East China; source attribution studies by ~~Ginoux et al. have revealed that large anthropogenic dust sources are found in these regions~~ Ginoux et al. (2012) have revealed that large anthropogenic dust sources are found in these regions. In the future, it is important that longer term measurements are carried out at the Bachok research station, to provide confirmation that dust episodes in these regions of Asia are responsible for the elevated levels of *nss*Ca^{2+} and other associated ions. Dust is one of the most abundant types of aerosol in the atmosphere and can have important impacts on both air quality and climate, therefore it is important that seasonal and annual trends in water-soluble ions are studied in more detail at the Bachok research station.

4 Conclusions

An accurate and reliable technique relying on ion chromatography has been used to make time-resolved measurements of water-soluble ions in atmospheric aerosol at the Bachok Marine and Atmospheric research station. Using meteorological data from the nearby airport, and HYSPLIT backward air mass trajectories centred on the Bachok research station, it was possible to observe both the diurnal wind pattern behaviour, and assess where the air masses arriving at the site originated from. Air quality at this remote location is influenced by local anthropogenic and biogenic emissions, as well as marine air masses from the South China Sea and aged emissions transported from highly polluted East Asian regions during the winter monsoon season. In general, the site was influenced by south westerlies coming from the land from the early hours of the morning until approximately 11 am, and then a dramatic shift in wind direction occurred and a sea breeze was present for the remainder of the day. This shift was accompanied by a drop in the concentrations of NO_x and anthropogenic VOCs (Dunmore et al., 2016).

Twelve atmospheric water-soluble ions were measured in this study and SO_4^{2-} was found to be the most dominant ion present, making up 66% of the total measured ion content on average. The non-sea salt and sea salt components of SO_4^{2-}, Na^+, K^+ and Ca^{2+} were determined, and it was found that 96% of the measured SO_4^{2-} was non-sea salt SO_4^{2-}. Predictions of aerosol pH were made using the ISOROPPIA-II thermodynamic model and it was estimated that the aerosol was highly acidic, with pH values ranging from -0.97 to 1.12; such levels of acidity are likely to have a detrimental impact on human health and the health of ecosystems at this remote coastal location. A clear difference in aerosol composition was found between continental air masses originating from industrialised regions of East Asia and marine air masses predominantly influenced by the South China Sea. For example, elevated SO_4^{2-} concentrations were observed when continental air masses that had passed over highly industrialised regions of East Asia arrived at the measurement site.

Correlation analyses amongst ionic species and assessment of ratios between different ions provided an insight into common sources and formation pathways of key atmospheric ions. Oxalate concentrations were recorded and found to be more comparable to measurements made at urban locations rather than rural ones. A strong correlation of $C_2O_4^{2-}$ with SO_4^{2-} suggested a common aqueous oxidation formation pathway. Strong correlation between $C_2O_4^{2-}$ and K^+ coupled with high $C_2O_4^{2-}/nssK^+$ ratios indicated that biomass burning was an important secondary source of oxalate in the Bachok region, whereas lack of correlation with NO_2^- and NO_3^- suggested that vehicular emissions were not an important source. The average $Cl^-/ssNa^+$ molar ratio during the measurement campaign was 0.40, significantly lower than that of bulk seawater (1.18). Analysis of back trajectories revealed that chloride depletion was greater when the aerosol was more influenced by anthropogenic sources of pollution. Elevated levels of $nssCa^{2+}$ and other ions such as PO_4^{3-}, Mg^{2+} and $nssNa^+$ were observed between midday on 30-01-2014 and midnight on 31-01-2014. Assuming that $nssCa^{2+}$ can be used as a tracer for atmospheric dust, it was proposed that the increased concentrations were a result of air masses arriving at the site from the North China Plains and Horqin Sandy Lands. Longer term measurements are required to fully investigate the influence of Asian dusts at this remote coastal location.

To our knowledge, time-resolved measurements of water-soluble ions in $PM_{2.5}$ are virtually non-existent in rural locations on the east coast of Peninsular Malaysia. The data presented in this study has demonstrated the capabilities of the new atmospheric tower at the Bachok research station and has provided an initial insight into factors affecting aerosol composition on this coastline. In the future, it is important that longer term measurements are carried out, with increased time-resolved sampling and particle size fractionation, to provide a better understanding of the factors affecting aerosol composition at this measurement site. This remote location is susceptible to the effects of local, regional and international air pollution, and rapid industrialisation in East Asia is influencing air quality along the east coast of Peninsular Malaysia.

Data availability. Raw data is available on PURE (DOI: 10.15124/bd4a9045-832b-4ff8-aecc-ef1653603f1d).

Author contribution. All authors contributed to the final version of this article. Naomi J Farren analysed the aerosol samples and wrote the paper under the supervision of Jacqueline F Hamilton. Rachel E Dunmore collected the aerosol samples. M Iqbal Mead, Mohd Shahrul Mohd Nadzir, Azizan Abu Samah and Siew-Moi Phang coordinate and manage the University of Malaya BMRS. William T Sturges coordinated the Bachok demonstration 'International Opportunities Fund' campaign.

Competing interests. The authors declare that they have no conflict of interest.

Acknowledgements. The financial support of the Natural Environment Research Council (N. Farren, PhD studentship NE/L501751/1) is gratefully acknowledged. N. Farren would like to thank David Carslaw for his assistance using Openair. All authors would like to acknowledge NERC (NE/J016012/1 and NE/J016047/1) for funding the Bachok demonstration 'International Opportunities Fund' campaign and HICoE-MoHE IOES-2014 (Air-Ocean-Land Interactions) for supporting the Bachok Marine Research Station facilities.

References

Ashfold, M. J., Latif, M. T., Samah, A. A., Mead, M. I., and Harris, N. R. P.: Influence of Northeast Monsoon cold surges on air quality in Southeast Asia, Atmos. Environ., 166, 498-509, 10.1016/j.atmosenv.2017.07.047, 2017.

Becagli, S., Proposito, M., Benassai, S., Gragnani, R., Magand, O., Traversi, R., and Udisti, R.: Spatial distribution of biogenic sulphur compounds (MSA, nssSO(4)(2-)) in the northern Victoria Land-Dome C-Wilkes Land, area, East Antarctica, Ann Glaciol, 41, 23-31, Doi 10.3189/172756405781813384, 2005.

Behrenfeld, M. J., O'Malley, R. T., Siegel, D. A., McClain, C. R., Sarmiento, J. L., Feldman, G. C., Milligan, A. J., Falkowski, P. G., Letelier, R. M., and Boss, E. S.: Climate-driven trends in contemporary ocean productivity, Nature, 444, 752-755, 10.1038/nature05317, 2006.

Bloss, W. J., Evans, M. J., Lee, J. D., Sommariva, R., Heard, D. E., and Pilling, M. J.: The oxidative capacity of the troposphere: Coupling of field measurements of OH and a global chemistry transport model, Faraday Discuss, 130, 425-436, 10.1039/b419090d, 2005.

Boreddy, S. K. R., Kawamura, K., and Jung, J. S.: Hygroscopic properties of particles nebulized from water extracts of aerosols collected at Chichijima Island in the western North Pacific: An outflow region of Asian dust, J Geophys Res-Atmos, 119, 167-178, 10.1002/2013JD020626, 2014.

Boreddy, S. K. R., and Kawamura, K.: A 12-year observation of water-soluble ions in TSP aerosols collected at a remote marine location in the western North Pacific: an outflow region of Asian dust, Atmos Chem Phys, 15, 6437-6453, 10.5194/acp-15-6437-2015, 2015.

Bowen, H. J. M.: Environmental chemistry of the elements, Academic Press, London, 1979.

Carlton, A. G., Turpin, B. J., Lim, H. J., Altieri, K. E., and Seitzinger, S.: Link between isoprene and secondary organic aerosol (SOA): Pyruvic acid oxidation yields low volatility organic acids in clouds, Geophys Res Lett, 33, Artn L06822 10.1029/2005gl025374, 2006.

Carpenter, L. J., Fleming, Z. L., Read, K. A., Lee, J. D., Moller, S. J., Hopkins, J. R., Purvis, R. M., Lewis, A. C., Muller, K., Heinold, B., Herrmann, H., Fomba, K. W., van Pinxteren, D., Muller, C., Tegen, I., Wiedensohler, A., Muller, T., Niedermeier, N., Achterberg, E. P., Patey, M. D., Kozlova, E. A., Heimann, M., Heard, D. E., Plane, J. M. C., Mahajan, A., Oetjen, H., Ingham, T., Stone, D., Whalley, L. K., Evans, M. J., Pilling, M. J., Leigh, R. J., Monks, P. S., Karunaharan, A., Vaughan, S., Arnold, S. R., Tschritter, J., Pohler, D., Friess, U., Holla, R., Mendes, L. M., Lopez, H., Faria, B., Manning, A. J., and Wallace, D. W. R.: Seasonal characteristics of tropical marine boundary layer air measured at the Cape Verde Atmospheric Observatory, J Atmos Chem, 67, 87-140, 10.1007/s10874-011-9206-1, 2010.

Carslaw, D. C., and Ropkins, K.: openair - An R package for air quality data analysis, Environ Modell Softw, 27-28, 52-61, 10.1016/j.envsoft.2011.09.008, 2012.

Carslaw, D. C.: The openair manual - open-source tools for analysing air pollution data. Manual for version 1.1-4., King's College London, 2015.

Charlson, R. J., Langner, J., Rodhe, H., Leovy, C. B., and Warren, S. G.: Perturbation of the Northern-Hemisphere Radiative Balance by Backscattering from Anthropogenic Sulfate Aerosols, Tellus A, 43, 152-163, DOI 10.1034/j.1600-0870.1991.00013.x, 1991.

Dominick, D., Latif, M. T., Juneng, L., Khan, M. F., Amil, N., Mead, M. I., Nadzir, M. S. M., Moi, P. S., Abu Samah, A., Ashfold, M. J., Sturges, W. T., Harris, N. R. P., Robinson, A. D., and Pyle, J. A.: Characterisation of particle mass and number concentration on the east coast of the Malaysian Peninsula during the northeast monsoon, Atmos. Environ., 117, 187-199, 10.1016/j.atmosenv.2015.07.018, 2015.

Draxler, R. R., and Hess, G. D.: Description of the HYSPLIT_4 modeling system, NOAA Air Resources Laboratory, Silver Spring, MD, NOAA Tech. Memo. ERL ARL-224, 24, 1997.

Draxler, R. R., and Hess, G. D.: An overview of the HYSPLIT_4 modeling system of trajectories, dispersion, and deposition, Aust. Meteor. Mag., 47, 295-308, 1998.

Draxler, R. R.: HYSPLIT4 user's guide, NOAA Air Resources Laboratory, Silver Spring, MD, NOAA Tech. Memo. ERL ARL-230, 1999.

Dunmore, R. E., Hopkins, J. R., Lidster, R. T., Mead, M. I., Bandy, B. J., Forster, G., Oram, D. E., Sturges, W. T., Phang, S. M., Abu Samah, A., and Hamilton, J. F.: Development of a Combined Heart-Cut and Comprehensive Two-Dimensional Gas Chromatography System to Extend the Carbon Range of Volatile Organic Compounds Analysis in a Single Instrument, Separations, 3, ARTN 21 10.3390/separations3030021, 2016.

EDGAR - Emissions Database for Global Atmospheric Research: http://edgar.jrc.ec.europa.eu/overview.php?v=431, access: 09-04-2017, 2016.

EPA, Title 40 Protection of Environment Part 136 Guidelines Establishing Test Procedures for the Analysis of Pollutants. In *Electronic Code of Federal Regulations* [Online] U.S. Government Publishing Office: Washington, DC, 2017. https://www.ecfr.gov/cgi-bin/text-idx?SID=57d5771415f8a36cb8c0e2ca2a1583a2&mc=true&node=pt40.25.136&rgn=div5#ap40.25.136_17.b (accessed 20-07-2017).

Facchini, M. C., Mircea, M., Fuzzi, S., and Charlson, R. J.: Cloud albedo enhancement by surface-active organic solutes in growing droplets, Nature, 401, 257-259, Doi 10.1038/45758, 1999.

Fisher, J. A., Jacob, D. J., Wang, Q. Q., Bahreini, R., Carouge, C. C., Cubison, M. J., Dibb, J. E., Diehl, T., Jimenez, J. L., Leibensperger, E. M., Lu, Z. F., Meinders, M. B. J., Pye, H. O. T., Quinn, P. K., Sharma, S., Streets, D. G., van Donkelaar, A., and Yantosca, R. M.: Sources, distribution, and acidity of sulfate-ammonium aerosol in the Arctic in winter-spring, Atmos. Environ., 45, 7301-7318, 10.1016/j.atmosenv.2011.08.030, 2011.

Fountoukis, C., and Nenes, A.: ISORROPIA II: a computationally efficient thermodynamic equilibrium model for K+-Ca2+-Mg2+-Nh(4)(+)-Na+-SO42--NO3--Cl--H2O aerosols, Atmos Chem Phys, 7, 4639-4659, 2007.

Freitas, A. D., Martins, L. D., and Solci, M. C.: Size-Segregated Particulate Matter and Carboxylic Acids over Urban and Rural Sites in Londrina City, Brazil, J Brazil Chem Soc, 23, 921-930, 2012.

Garreaud, R. D.: Subtropical cold surges: Regional aspects and global distribution, Int J Climatol, 21, 1181-1197, Doi 10.1002/Joc.687, 2001.

Global Atmospheric Watch Station Information System (GAWSIS): https://gawsis.meteoswiss.ch/GAWSIS//index.html#/, access: 12-04-2017, 2017.

Ginoux, P., Prospero, J. M., Gill, T. E., Hsu, N. C., and Zhao, M.: Global-Scale Attribution of Anthropogenic and Natural Dust Sources and Their Emission Rates Based on Modis Deep Blue Aerosol Products, Rev Geophys, 50, Artn Rg3005 10.1029/2012rg000388, 2012.

Location of GAW sites in the Maritime Continent: https://www.google.com/maps/d/edit?hl=en&mid=1YfjfFiFfY5joJai4ymtLz-4PP3o&ll=7.027578969175066%2C110.68402862549999&z=5, access: 07-12-2017, 2017.

Gwynn, R. C., Burnett, R. T., and Thurston, G. D.: A time-series analysis of acidic particulate matter and daily mortality and morbidity in the Buffalo, New York, region, Environ Health Persp, 108, 125-133, Doi 10.2307/3454510, 2000.

Hennigan, C. J., Izumi, J., Sullivan, A. P., Weber, R. J., and Nenes, A.: A critical evaluation of proxy methods used to estimate the acidity of atmospheric particles, Atmos Chem Phys, 15, 2775-2790, 10.5194/acp-15-2775-2015, 2015.

Huang, X. F., Yu, J. Z., He, L. Y., and Yuan, Z. B.: Water-soluble organic carbon and oxalate in aerosols at a coastal urban site in China: Size distribution characteristics, sources, and formation mechanisms, J Geophys Res-Atmos, 111, Artn D22212

10.1029/2006jd007408, 2006.

Huang, X. F., and Yu, J. Z.: Is vehicle exhaust a significant primary source of oxalic acid in ambient aerosols?, Geophys Res Lett, 34, Artn L02808

10.1029/2006gl028457, 2007.

Ismail, M., Yuen, F. S., and Abdullah, S. S.: Particulate Matter Status and its Relationship with Meteorological Factors in the East Coast of Peninsular Malaysia, Journal of Engineering and Applied Sciences, 11, 2588-2593, 2016.

Jiang, Y., Zhuang, G., Wang, Q., Liu, T., Huang, K., Fu, J. S., Li, J., Lin, Y., Zhang, R., and Deng, C.: Characteristics, sources and formation of aerosol oxalate in an Eastern Asia megacity and its implication to haze pollution, Atmos Chem Phys Discuss, 11, 22075-22112, 10.5194/acpd-11-22075-2011, 2011.

Kerminen, V. M.: Relative roles of secondary sulfate and organics in atmospheric cloud condensation nuclei production, J Geophys Res-Atmos, 106, 17321-17333, Doi 10.1029/2001jd900204, 2001.

Keywood, M. D., Ayers, G. P., Gras, J. L., Boers, R., and Leong, C. P.: Haze in the Klang Valley of Malaysia, Atmos Chem Phys, 3, 591-605, 2003.

Lawrence, M. G., Jockel, P., and von Kuhlmann, R.: What does the global mean OH concentration tell us?, Atmos Chem Phys, 1, 37-49, 2001.

Legrand, M., and Pasteur, E. C.: Methane sulfonic acid to non-sea-salt sulfate ratio in coastal Antarctic aerosol and surface snow, J Geophys Res-Atmos, 103, 10991-11006, Doi 10.1029/98jd00929, 1998.

Lin, Y. H., Zhang, Z. F., Docherty, K. S., Zhang, H. F., Budisulistiorini, S. H., Rubitschun, C. L., Shaw, S. L., Knipping, E. M., Edgerton, E. S., Kleindienst, T. E., Gold, A., and Surratt, J. D.: Isoprene Epoxydiols as Precursors to Secondary Organic Aerosol Formation: Acid-Catalyzed Reactive Uptake Studies with Authentic Compounds, Environ. Sci. Technol., 46, 250-258, 10.1021/es202554c, 2012.

Murphy, J. G., Gregoire, P. K., Tevlin, A. G., Wentworth, G. R., Ellis, R. A., Markovic, M. Z., and Vandenboer, T. C.: Observational constraints on particle acidity using measurements and modelling of particles and gases, Faraday Discuss, xx, 1-17, 2017.

Myriokefalitakis, S., Tsigaridis, K., Mihalopoulos, N., Sciare, J., Nenes, A., Kawamura, K., Segers, A., and Kanakidou, M.: In-cloud oxalate formation in the global troposphere: a 3-D modeling study, Atmos Chem Phys, 11, 5761-5782, 10.5194/acp-11-5761-2011, 2011.

Neale, R., and Slingo, J.: The maritime continent and its role in the global climate: A GCM study, J Climate, 16, 834-848, Doi 10.1175/1520-0442(2003)016<0834:Tmcair>2.0.Co;2, 2003.

Newberg, J. T., Matthew, B. M., and Anastasio, C.: Chloride and bromide depletions in sea-salt particles over the northeastern Pacific Ocean, J Geophys Res-Atmos, 110, Artn D06209

10.1029/2004jd005446, 2005.

National Oceanic and Atmospheric Administration Integrated Surface Database https://www.ncdc.noaa.gov/isd, access: 20-07-2017, 2003.

Novakov, T., and Penner, J. E.: Large Contribution of Organic Aerosols to Cloud-Condensation-Nuclei Concentrations, Nature, 365, 823-826, Doi 10.1038/365823a0, 1993.

Oram, D. E., Ashfold, M. J., Laube, J. C., Gooch, L. J., Humphrey, S., Sturges, W. T., Leedham-Elvidge, E., Forster, G. L., Harris, N. R. P., Mead, M. I., Abu Samah, A., Phang, S. M., Ou-Yang, C. F., Lin, N. H., Wang, J. L., Baker, A. K., Brenninkmeijer, C. A. M., and Sherry, D.: A growing threat to the ozone layer from short-lived anthropogenic chlorocarbons, Atmos Chem Phys, 17, 11929-11941, 10.5194/acp-17-11929-2017, 2017.

Pyle, J. A., Ashfold, M. J., Harris, N. R. P., Robinson, A. D., Warwick, N. J., Carver, G. D., Gostlow, B., O'Brien, L. M., Manning, A. J., Phang, S. M., Yong, S. E., Leong, K. P., Ung, E. H., and Ong, S.: Bromoform in the tropical boundary layer of the Maritime Continent during OP3, Atmos Chem Phys, 11, 529-542, 10.5194/acp-11-529-2011, 2011.

Ripp, J.: Analytical Detection Limit Guidance and Laboratory Guide for Determining Method Detection Limits, Wisconsin Department of Natural Resources, Madison, WI, PUBL-TS-056-96, 1996.

Robinson, A. D., Harris, N. R. P., Ashfold, M. J., Gostlow, B., Warwick, N. J., O'Brien, L. M., Beardmore, E. J., Nadzir, M. S. M., Phang, S. M., Samah, A. A., Ong, S., Ung, H. E., Peng, L. K., Yong, S. E., Mohamad, M., and Pyle, J. A.: Long-term halocarbon observations from a coastal and an inland site in Sabah, Malaysian Borneo, Atmos Chem Phys, 14, 8369-8388, 10.5194/acp-14-8369-2014, 2014.

Sareen, N., Carlton, A. G., Surratt, J. D., Gold, A., Lee, B., Lopez-Hilfiker, F. D., Mohr, C., Thornton, J. A., Zhang, Z. F., Lim, Y. B., and Turpin, B. J.: Identifying precursors and aqueous organic aerosol formation pathways during the SOAS campaign, Atmos Chem Phys, 16, 14409-14420, 10.5194/acp-16-14409-2016, 2016.

Savoie, D. L., and Prospero, J. M.: Comparison of Oceanic and Continental Sources of Non-Sea-Salt Sulfate over the Pacific-Ocean, Nature, 339, 685-687, Doi 10.1038/339685a0, 1989.

Saxena, P., and Hildemann, L. M.: Water-soluble organics in atmospheric particles: A critical review of the literature and application of thermodynamics to identify candidate compounds, J Atmos Chem, 24, 57-109, Doi 10.1007/Bf00053823, 1996.

Seinfeld, J. H., and Pandis, S. N.: Atmospheric chemistry and physics : from air pollution to climate change, 2nd ed., J. Wiley, Hoboken, N.J., 1-1203 pp., 2006.

Sempere, R., and Kawamura, K.: Comparative Distributions of Dicarboxylic-Acids and Related Polar Compounds in Snow Rain and Aerosols from Urban Atmosphere, Atmos. Environ., 28, 449-459, Doi 10.1016/1352-2310(94)90123-6, 1994.

Stein, A. F., Draxler, R. R., Rolph, G. D., Stunder, B. J. B., Cohen, M. D., and Ngan, F.: Noaa's Hysplit Atmospheric Transport and Dispersion Modeling System, Bulletin of the American Meteorological Society, 96, 2059-2077, 10.1175/Bams-D-14-00110.1, 2015.

Sturges, W. T., and Shaw, G. E.: Halogens in Aerosols in Central Alaska, Atmos Environ a-Gen, 27, 2969-2977, Doi 10.1016/0960-1686(93)90329-W, 1993.

Surratt, J. D., Chan, A. W. H., Eddingsaas, N. C., Chan, M. N., Loza, C. L., Kwan, A. J., Hersey, S. P., Flagan, R. C., Wennberg, P. O., and Seinfeld, J. H.: Reactive intermediates revealed in secondary organic aerosol formation from isoprene, PNAS, 107, 6640-6645, 10.1073/pnas.0911114107, 2010.

Tahir, N. M., Suratman, S., Fong, F. T., Hamzah, M. S., and Latif, M. T.: Temporal Distribution and Chemical Characterization of Atmospheric Particulate Matter in the Eastern Coast of Peninsular Malaysia, Aerosol Air Qual Res, 13, 584-595, 10.4209/aaqr.2012.08.0216, 2013.

Tan, Y., Lim, Y. B., Altieri, K. E., Seitzinger, S. P., and Turpin, B. J.: Mechanisms leading to oligomers and SOA through aqueous photooxidation: insights from OH radical oxidation of acetic acid and methylglyoxal, Atmos Chem Phys, 12, 801-813, 10.5194/acp-12-801-2012, 2012.

Taylor, S. R.: Abundance of Chemical Elements in the Continental Crust - a New Table, Geochim Cosmochim Ac, 28, 1273-1285, Doi 10.1016/0016-7037(64)90129-2, 1964.

Yamasoe, M. A., Artaxo, P., Miguel, A. H., and Allen, A. G.: Chemical composition of aerosol particles from direct emissions of vegetation fires in the Amazon Basin: water-soluble species and trace elements, Atmos. Environ., 34, 1641-1653, Doi 10.1016/S1352-2310(99)00329-5, 2000.

Zhang, Y., Sperber, K. R., and Boyle, J. S.: Climatology and interannual variation of the East Asian winter monsoon: Results from the 1979-95 NCEP/NCAR reanalysis, Mon Weather Rev, 125, 2605-2619, Doi 10.1175/1520-0493(1997)125<2605:Caivot>2.0.Co;2, 1997.

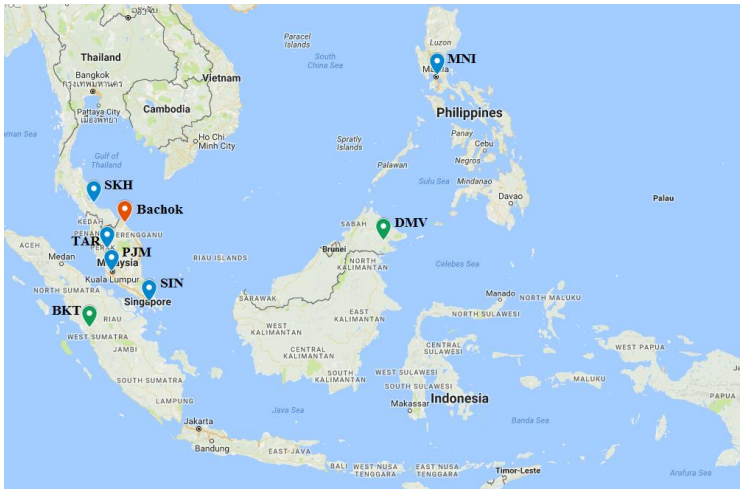

Figure 1: Location of global (green pins) and regional (blue pins) GAW sites in the Maritime Continent; Danum Valley in Malaysia (DMV), Bukit Kototabang in Indonesia (BKT), Manila in Philippines (MNI), Songkhla in Thailand (SKH), Tanah Rata in Malaysia (TAR), Petaling Jaya in Malaysia (PJM) and Singapore (SIN) (gawsis.ch, 2017). The red pin shows the location of the Bachok Marine and Atmospheric Research Station. Map created using google maps (google.com, 2017).

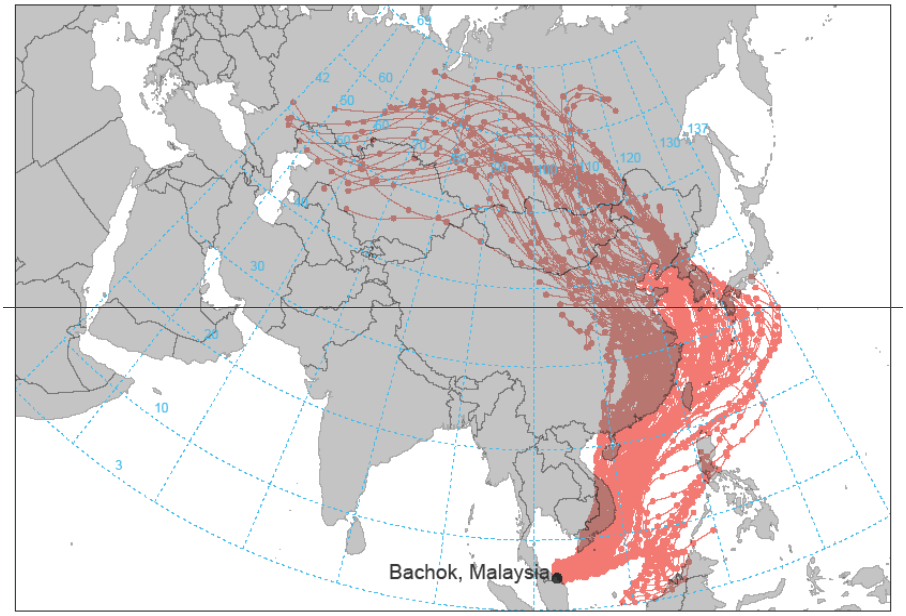
Bachok, Malaysia

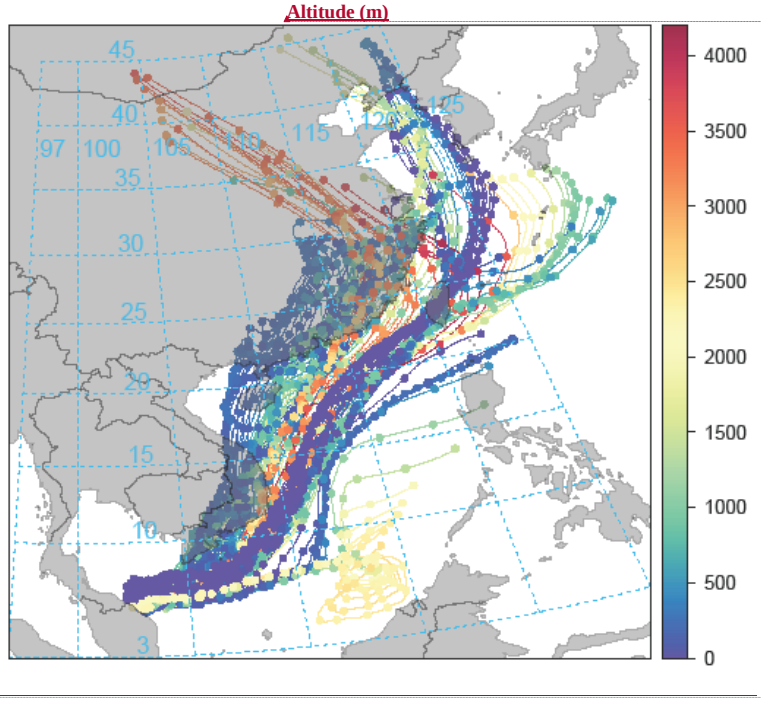

Field Code Changed

Formatted: Font: Bold

Figure 2: ~~107~~-day HYSPLIT backward air mass trajectories centred on the Bachok Marine and Atmospheric Research Station between 18-01-2014 and 07-02-2014. The back trajectories are coloured by the altitude of the air mass (m). Plot constructed using the openair package in RStudio (Carslaw and Ropkins, 2012; Carslaw, 2015).

Table 1: Mean and maximum ion concentrations measured throughout the measurement period. The average % mass contribution of each ion to the total measured ions is included, as well as the % of samples in which each target ion is found (%Qt).

Ion	Mean [ion] / µg m^{-3}	Maximum [ion] / µg m^{-3}	Mean % mass of total measured ion content	%Qt[a]	%RSD$_{total}$[b]
SO_4^{2-}	10.7	20.8	65.6	100	11.2
NH_4^+	1.69	4.73	10.4	100	6.38
Na^+	1.13	2.60	6.95	100	6.88
Cl^-	0.67	2.38	4.14	100	8.49
NO_3^-	0.61	1.52	3.76	100	22.6
$C_2O_4^{2-}$	0.42	0.65	2.57	97	13.9
PO_4^{3-}	0.36	2.34	2.22	93	15.4
K^+	0.38	0.67	0.67	100	6.35
Ca^{2+}	0.10	0.35	0.64	100	9.26
Mg^{2+}	0.10	0.21	0.61	100	6.72
$CH_3SO_3^-$	0.08	0.22	0.47	67	10.6
NO_2^-	0.05	0.16	0.33	23	14.3
Total	**16.2**	**27.0**	--	--	--

[a]Percentage of samples in which the target ion was above the LOQ. [b]Total error associated with each ion.

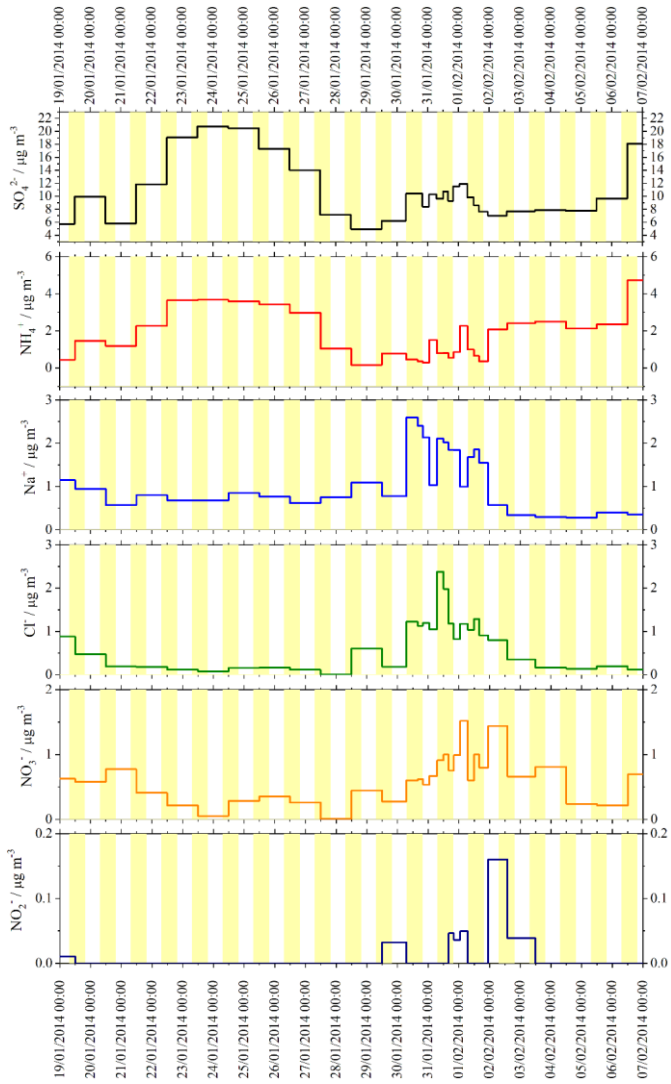

Figure 3: Time series of SO_4^{2-}, NH_4^+, Na^+, Cl^-, NO_3^- and NO_2^- concentration (µg m^{-3}) during the Bachok demonstration campaign (18-01-2014 to 07-02-2014). Yellow shaded areas represent the time between sunrise and sunset (local).

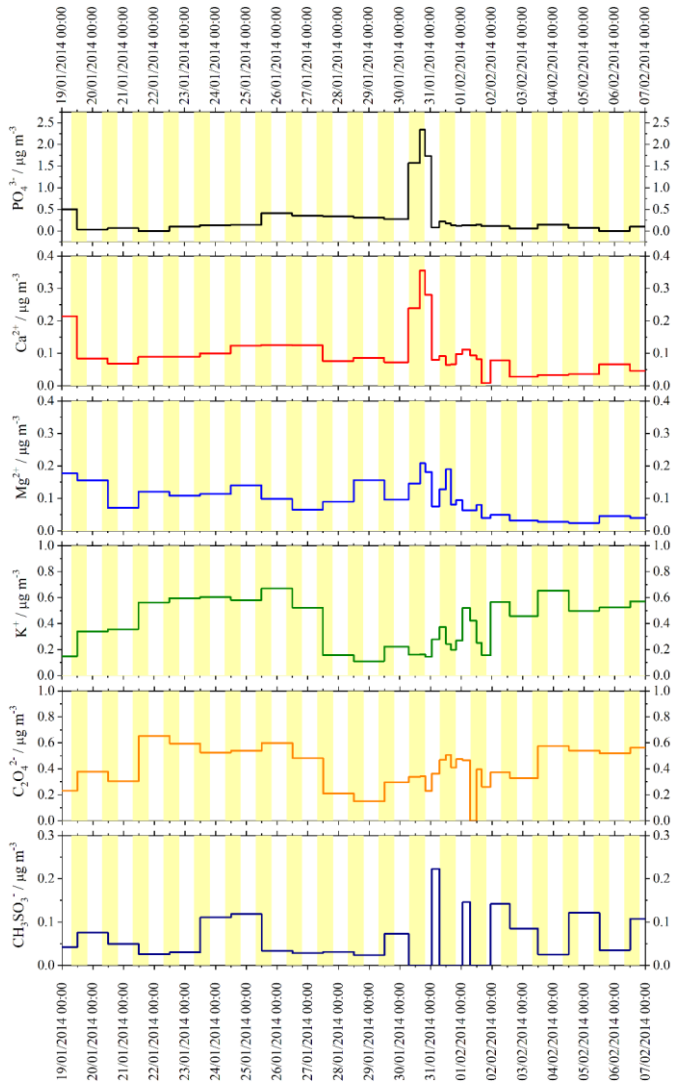

940 **Figure 4: Time series of PO_4^{3-}, Ca^{2+}, Mg^{2+}, K^+, $C_2O_4^{2-}$ and $CH_3SO_3^-$ concentration (µg m^{-3}) during the Bachok demonstration campaign (18-01-2014 to 07-02-2014). Yellow shaded areas represent the time between sunrise and sunset (local).**

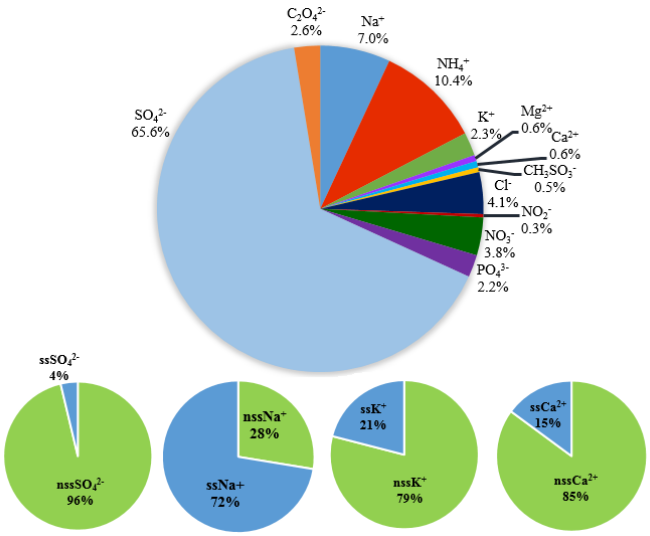

Figure 5: Pie chart to show the average mass composition of water-soluble ions in aerosol collected at the Bachok research station (upper panel) and pie charts to show the percentage of non-sea salt and sea salt fractions of Na^+, SO_4^{2-}, K^+, Ca^{2+} (lower panel, left to right).

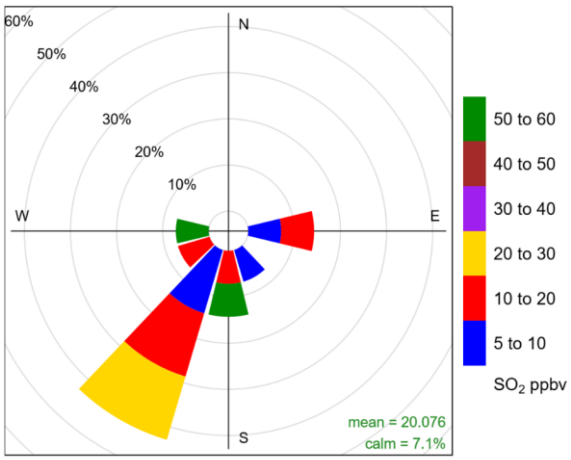

Figure 6: Pollution rose to show the relationship between wind direction and SO_2 concentration (≥ 5 ppb) at the Bachok measurement site. Plot constructed using the openair package in RStudio (Carslaw and Ropkins, 2012; Carslaw, 2015).

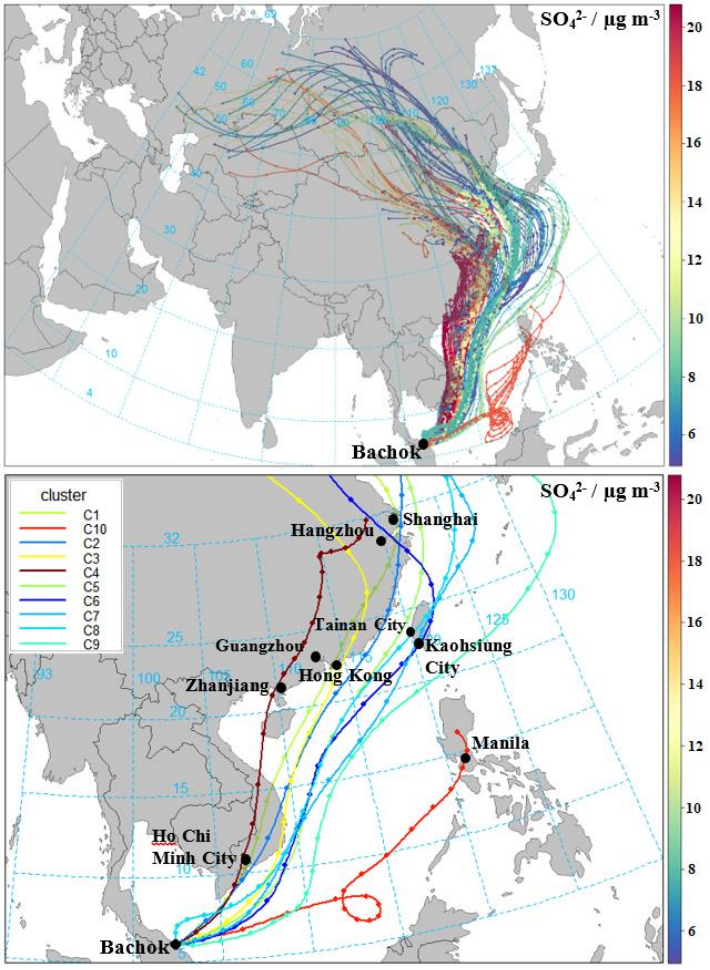
SO_4^{2-} / µg m^{-3}
20
18
16
14
12
10
8
6
Bachok
cluster
C1
C10
C2
C3
C4
C5
C6
C7
C8
C9
Hangzhou
Shanghai
Tainan City
Kaohsiung City
Guangzhou
Hong Kong
Zhanjiang
Manila
Ho Chi Minh City
Bachok

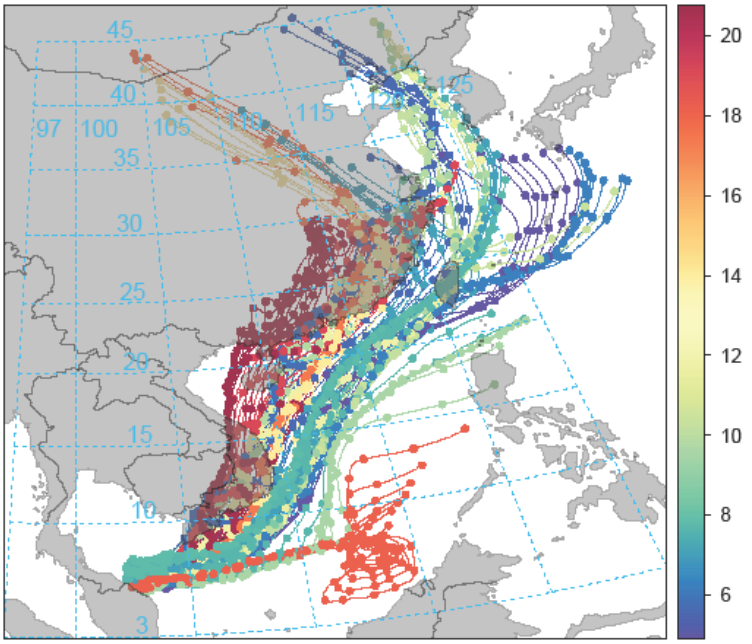

970 **Figure 7: ~~Upper panel shows 107~~-day HYSPLIT backward air mass trajectories centred on the Bachok research station between 18-01-2014 and 07-02-2014. The back trajectories are coloured by the concentration of SO_4^{2-} (µg m^{-3}). ~~Lower panel shows the 10 cluster solution to backward air mass trajectories centred on the Bachok research station during the same time period. The clusters are coloured by the average concentration of SO_4^{2-} (µg m^{-3}).~~ Plot constructed using the openair package in RStudio (Carslaw and Ropkins, 2012; Carslaw, 2015).**

Field Code Changed
Formatted: Font: Bold
Formatted: Font: Bold, Superscript
Formatted: Font: Bold
Formatted: Centered

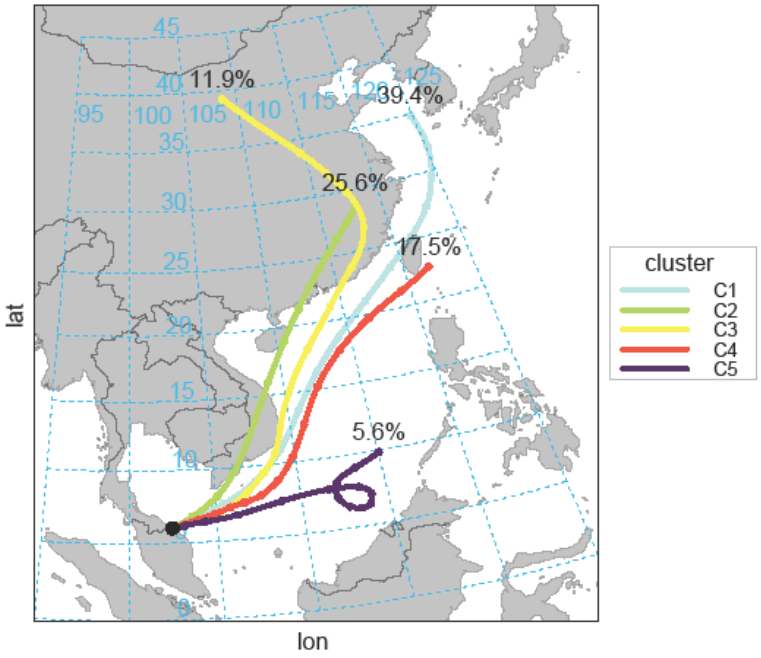

Figure 8: 5-cluster solution to backward air mass trajectories centred on the Bachok research station between 18-01-2014 and 07-02-2014. Plot constructed using the openair package in RStudio (Carslaw and Ropkins, 2012; Carslaw, 2015).

Field Code Changed

Formatted: Normal, Centered, Line spacing: single

Formatted: Justified

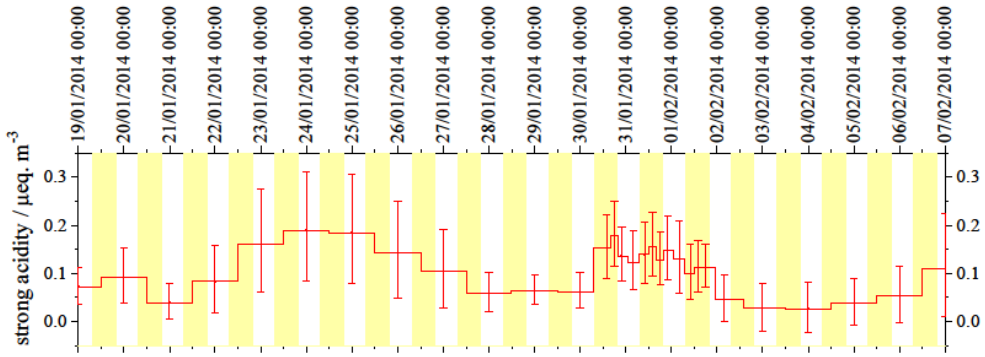

Figure 89: Particle strong acidity and associated error predictions for the aerosol collected during the Bachok measurement campaign. Yellow shaded areas represent the time between sunrise and sunset (local).

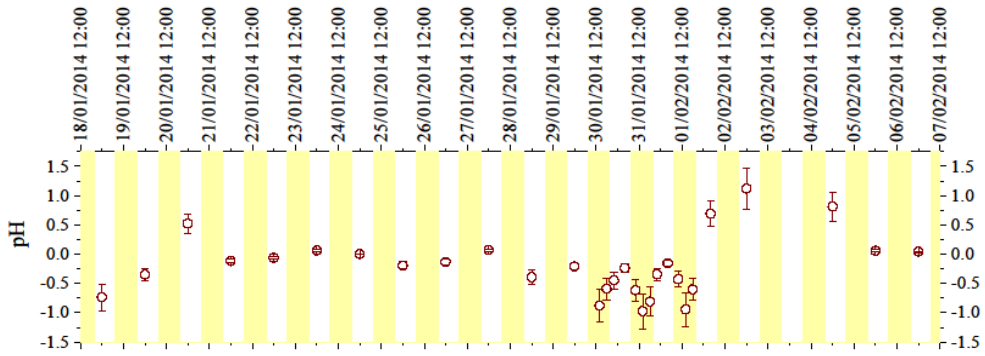

Figure 910: Predicted $PM_{2.5}$ pH at the Bachok measurement site using ISOROPPIA-II. Yellow shaded areas represent the time between sunrise and sunset (local).

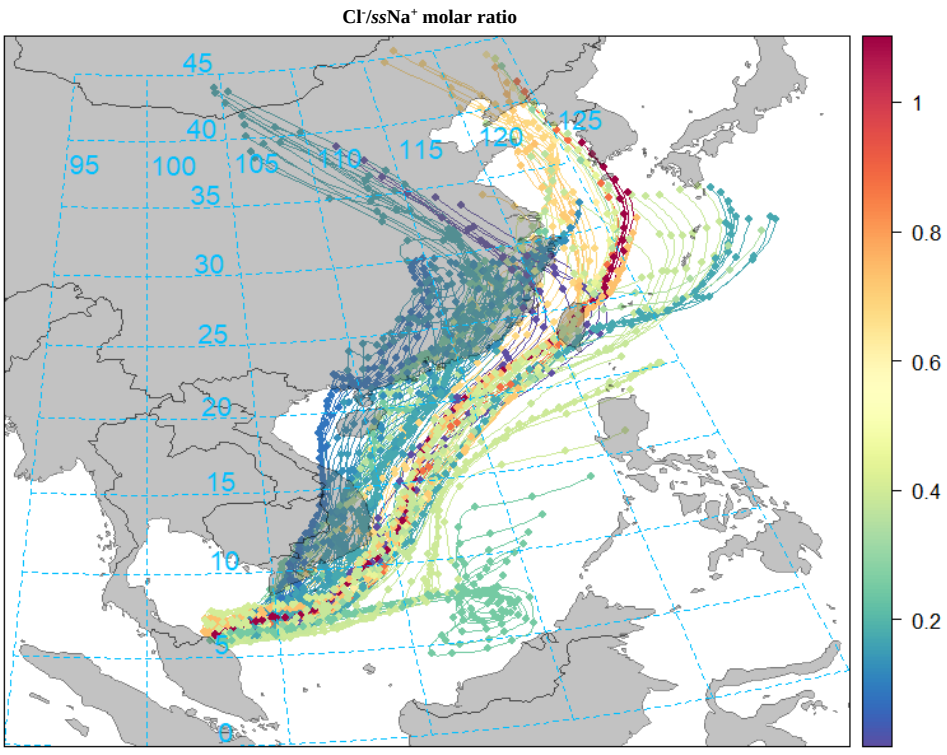
Cl⁻/ssNa⁺ molar ratio
45
40
35
30
25
20
15
10
5
0
95
100
105
110
115
120
125
1
0.8
0.6
0.4
0.2

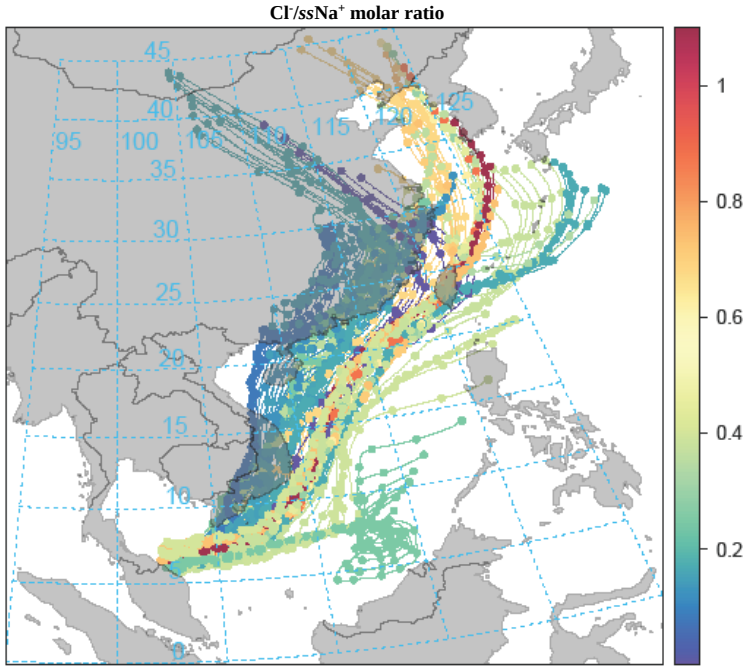

Field Code Changed

Figure ~~10~~11: ~~10~~7-day HYSPLIT back trajectories centred on the Bachok research station, between 18-01-2014 and 07-02-2014. The back trajectories are coloured by the $Cl^-/ssNa^+$ molar ratio. Plot constructed using the openair package in RStudio (Carslaw and Ropkins, 2012; Carslaw, 2015).

Table S1: Recovery levels of the extracted target ions and associated %RSD$_{rec}$ (n = 3). Procedural blank peak areas for each ion and average blank contribution to field samples over the entire sampling period are also shown.

Ion	% Recovery	%RSD$_{rec}$ (n = 3)	Blank area / µS min^{-1}	Average % blank contribution
Cl^-	79.5	2.9	3.31×10^{-3}	2.7
NO_2^-	81.5	3.2	not detected	not detected
NO_3^-	78.8	5.3	6.19×10^{-3}	7.6
PO_4^{3-}	98.2	5.6	2.38×10^{-2}	52.0
SO_4^{2-}	80.4	7.9	1.31×10^{-2}	1.0
$CH_3SO_3^-$	74.5	2.8	not detected	not detected
$C_2O_4^{2-}$	82.5	2.9	not detected	not detected
Na^+	87.3	6.0	6.51×10^{-1}	53.8
NH_4^+	80.0	4.6	2.03×10^{-2}	4.9
K^+	78.3	5.3	1.31×10^{-2}	12.5
Mg^{2+}	83.3	4.8	3.76×10^{-2}	26.1
Ca^{2+}	123.3	7.6	5.21×10^{-2}	34.0

Table S2: Instrumental parameters and associated errors for the IC.

Ion	RT range / min	LOD / ng	LOQ / ng	%RSD$_{ins}$ (n = 10)	%RSD$_{total}$
Cl^-	4.97 – 5.00	9.61	46.01	7.97	11.2
NO_2^-	5.86 – 5.89	5.47	25.25	22.36	6.38
NO_3^-	8.16 – 8.31	8.70	36.18	13.31	6.88
PO_4^{3-}	11.23 – 11.38	13.96	42.91	14.40	8.49
SO_4^{2-}	13.61 – 13.70	20.98	66.46	8.02	22.6
$CH_3SO_3^-$	4.50 – 4.53	6.16	29.47	10.26	13.9
$C_2O_4^{2-}$	15.72 – 15.85	9.99	144.18	13.58	15.4
Na^+	4.10 – 4.14	1.01	2.51	3.32	6.35
NH_4^+	4.64 – 4.68	0.77	2.96	4.38	9.26
K^+	5.71 – 5.77	1.65	2.79	3.55	6.72
Mg^{2+}	8.84 – 9.06	2.11	3.67	4.73	10.6
Ca^{2+}	10.99 – 11.28	0.47	6.14	5.32	14.3

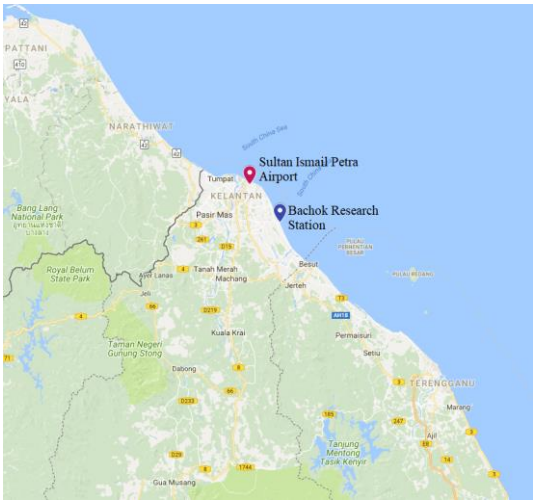

Figure S1: Map to show the location of the Sultan Ismail Petra airport, which is located 23 km away from the Bachok Research Station. Map created using google maps (google.com, 2017).

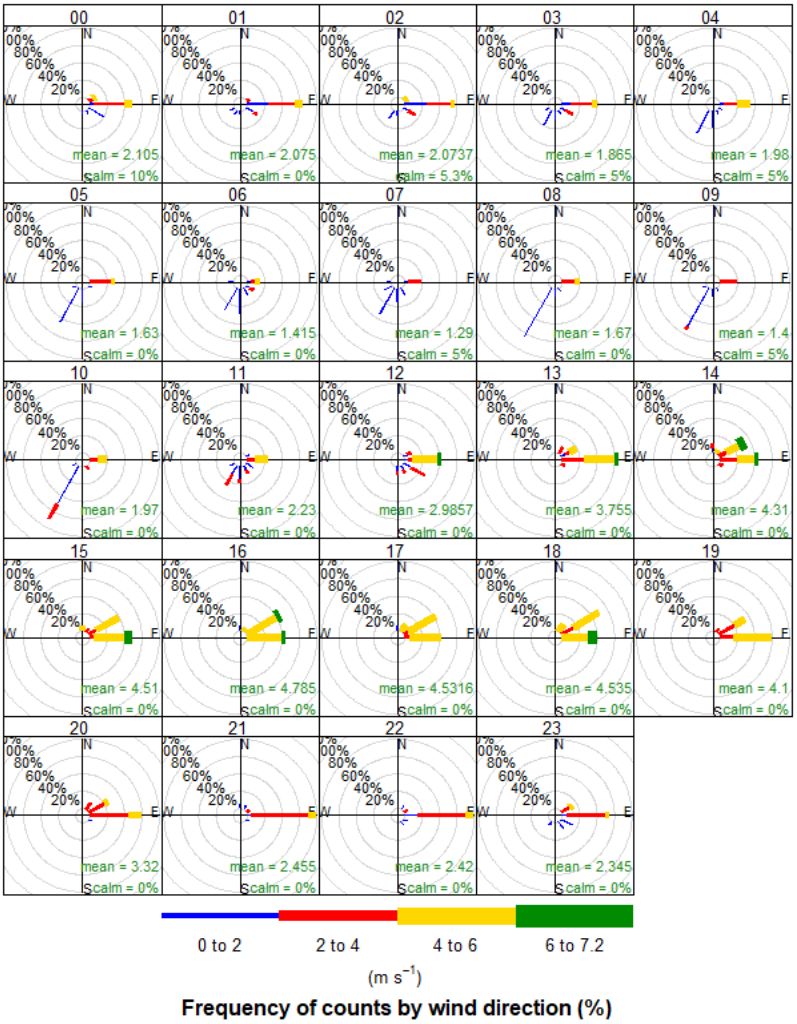

Figure S2: Wind rose plots to show hourly wind speed and wind direction averaged across the measurement campaign (18-01-2014 to 06-02-2014). Plot constructed using the openair package in RStudio (Carslaw and Ropkins, 2012; Carslaw, 2015).

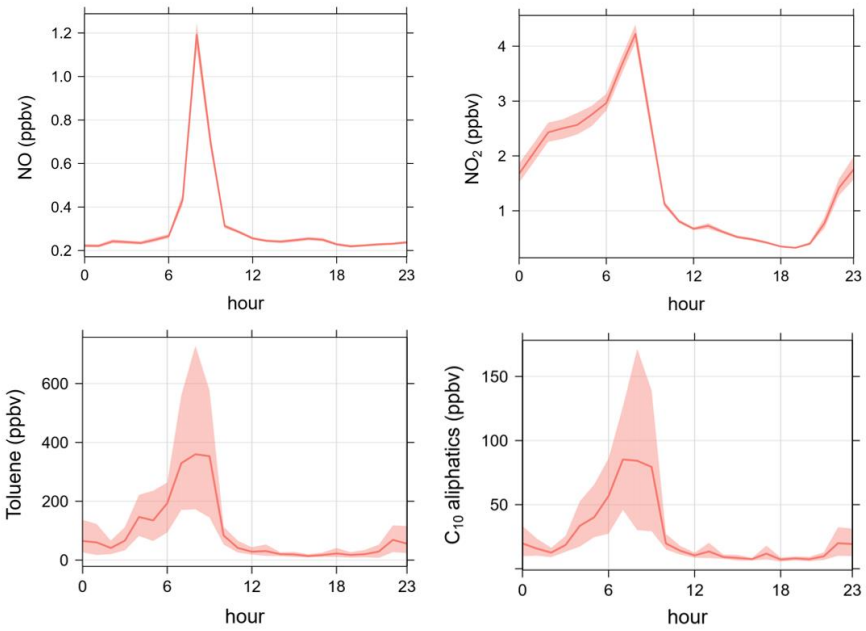

Figure S3: Diurnal profiles of NO, NO_2, toluene and C_{10} aliphatics measured using GC-GC×GC (Dunmore et al., 2016). The solid line represents the mean daily concentration and the shaded regions show the 95% confidence intervals surrounding the mean. Plot constructed using the openair package in RStudio (Carslaw and Ropkins, 2012; Carslaw, 2015).

Table S3: Average altitude, pressure and SO_4^{2-} concentration of air masses arriving at the Bachok measurement site within each cluster.

Cluster	Mean altitude (m)	Mean pressure (mbar)	Mean SO_4^{2-} (μg m^{-3})
1	169	991	8.4
2	65	991	14.4
3	501	944	13.8
4	37	1003	8.3
5	1000	899	18.1

Formatted: Normal, Line spacing: single

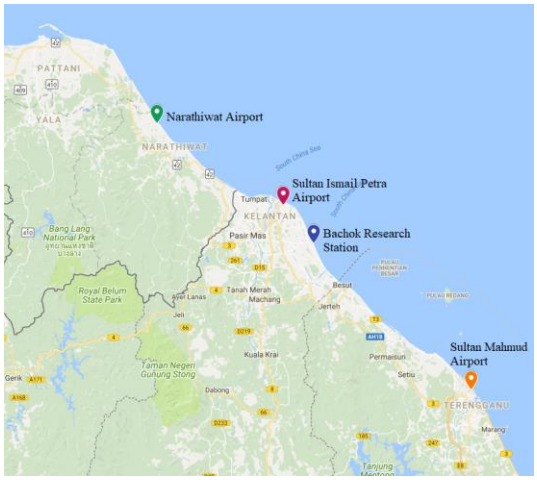

Figure S4: Map to show the location of Sultan Ismail Petra airport (23 km away), Narathiwat airport (102 km away) and Sultan Mahmud airport (103 km away) in relation to the Bachok Research Station. Map created using google maps (google.com, 2017).

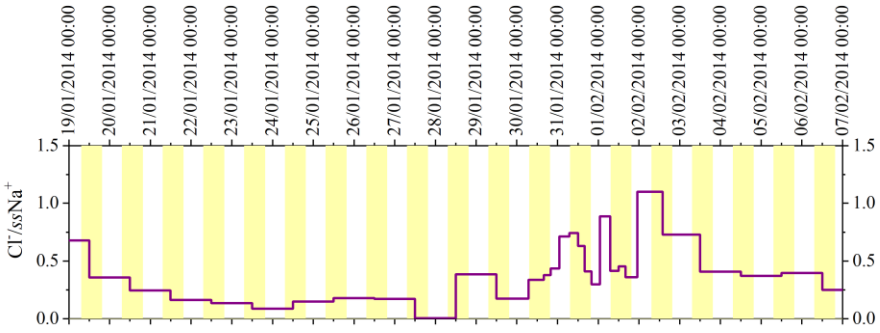

Figure S5: Time series of $Cl^-/ssNa^+$ molar ratio during the Bachok measurement campaign. Yellow shaded areas represent the time between sunrise and sunset (local).

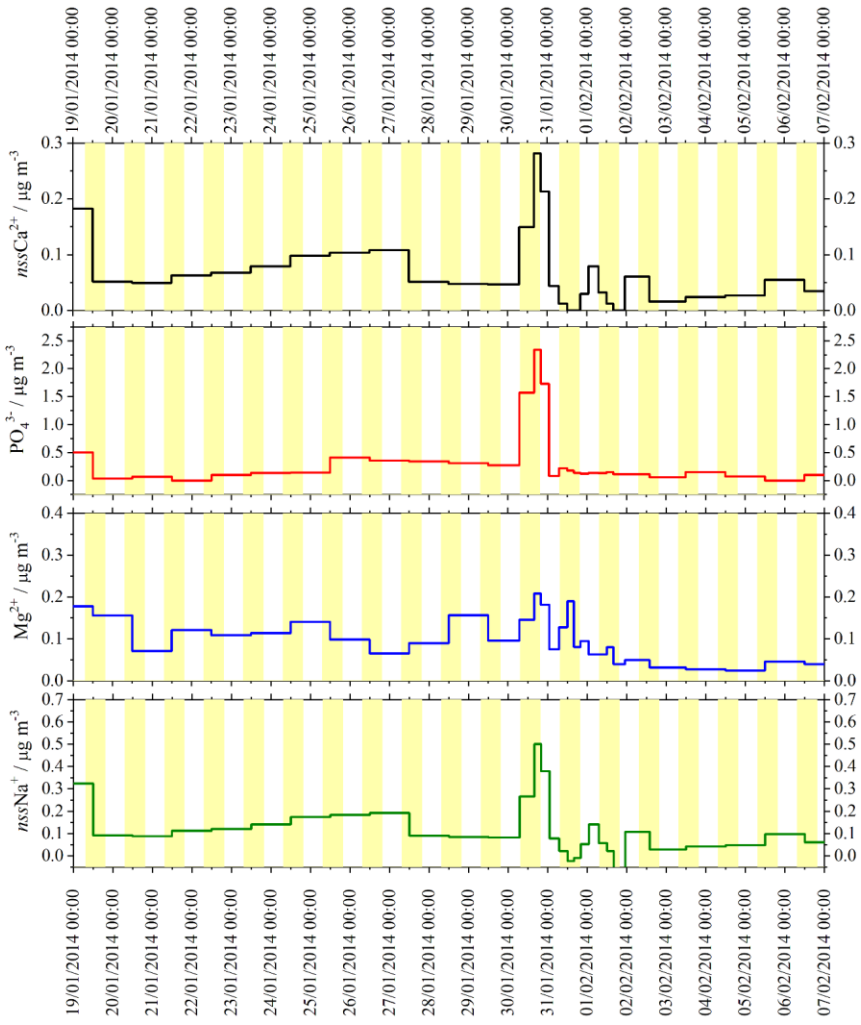

Figure S6: Time series of *nss*Ca^{2+}, PO_4^{3-}, Mg^{2+} and *nss*Na^{+} concentration (µg m^{-3}) during the Bachok measurement period (18-01-2014 to 07-02-2014). Yellow shaded areas represent the time between sunrise and sunset (local).